frontiers in Earth Science

ORIGINAL RESEARCH
published: 08 March 2018
doi: 10.3389/feart.2018.00015

Partial Melting of Lower Oceanic Crust Gabbro: Constraints From Poikilitic Clinopyroxene Primocrysts

Julien Leuthold[1], C. Johan Lissenberg[2], Brian O'Driscoll[3], Ozge Karakas[1], Trevor Falloon[4], Dina N. Klimentyeva[1] and Peter Ulmer[1]*

[1] Institute of Geochemistry and Petrology, Department of Earth Sciences, ETH Zürich, Zurich, Switzerland, [2] School of Earth and Ocean Sciences, Cardiff University, Cardiff, United Kingdom, [3] School of Earth and Environmental Sciences, University of Manchester, Manchester, United Kingdom, [4] School of Physical Sciences, Discipline of Earth Sciences, University of Tasmania, Hobart, TAS, Australia

Successive magma batches underplate, ascend, stall and erupt along spreading ridges, building the oceanic crust. It is therefore important to understand the processes and conditions under which magma differentiates at mid ocean ridges. Although fractional crystallization is considered to be the dominant mechanism for magma differentiation, open-system igneous complexes also experience Melting-Assimilation-Storage-Hybridization (MASH, Hildreth and Moorbath, 1988) processes. Here, we examine crystal-scale records of partial melting in lower crustal gabbroic cumulates from the slow-spreading Atlantic oceanic ridge (Kane Megamullion; collected with Jason ROV) and the fast-spreading East Pacific Rise (Hess Deep; IODP expedition 345). Clinopyroxene oikocrysts in these gabbros preserve marked intra-crystal geochemical variations that point to crystallization-dissolution episodes in the gabbro eutectic assemblage. Kane Megamullion and Hess Deep clinopyroxene core1 primocrysts and their plagioclase inclusions indicate crystallization from high temperature basalt (>1,160 and >1,200°C, respectively), close to clinopyroxene saturation temperature (<50% and <25% crystallization). Step-like compatible Cr (and co-varying Al) and incompatible Ti, Zr, Y and rare earth elements (REE) decrease from anhedral core1 to overgrown core2, while Mg# and Sr/Sr* ratios increase. We show that partial resorption textures and geochemical zoning result from partial melting of REE-poor lower oceanic crust gabbroic cumulate (protolith) following intrusion by hot primitive mantle-derived melt, and subsequent overgrowth crystallization (refertilization) from a hybrid melt. In addition, toward the outer rims of crystals, Ti, Zr, Y and the REE strongly increase and Al, Cr, Mg#, Eu/Eu*, and Sr/Sr* decrease, suggesting crystallization either from late-stage percolating relatively differentiated melt or from *in situ* trapped melt. Intrusion of primitive hot reactive melt and percolation of interstitial differentiated melt are two distinct MASH processes in the lower oceanic crust. They are potentially fundamental mechanisms for generating the wide compositional variation observed in mid-ocean ridge basalts. We furthermore propose that such processes operate at both slow- and fast-spreading ocean ridges.

OPEN ACCESS

Edited by:
Scott Andrew Whattam, Indian Institute of Technology Bhubaneswar, India

Reviewed by:
Ian Ernest Masterman Smith, University of Auckland, New Zealand
Sobhi Jaber Nasir, Sultan Qaboos University, Oman

***Correspondence:**
Julien Leuthold
julien.leuthold@erdw.ethz.ch

Specialty section:
This article was submitted to Petrology, a section of the journal Frontiers in Earth Science

Received: *01 December 2017*
Accepted: *12 February 2018*
Published: *08 March 2018*

Citation:
Leuthold J, Lissenberg CJ, O'Driscoll B, Karakas O, Falloon T, Klimentyeva DN and Ulmer P (2018) Partial Melting of Lower Oceanic Crust Gabbro: Constraints From Poikilitic Clinopyroxene Primocrysts. Front. Earth Sci. 6:15. doi: 10.3389/feart.2018.00015

Thermal numerical modeling shows that the degree of lower crustal partial melting at slow-spreading ridges can locally increase up to 50%, but the overall crustal melt volume is low (less than ca. 5% of total mantle-derived and crustal melts; ca. 20% in fast-spreading ridges).

Keywords: spreading ridge, lower oceanic crust, partial melting, poikilitic gabbro, clinopyroxene, primocryst, zoning, MORB petrogenesis

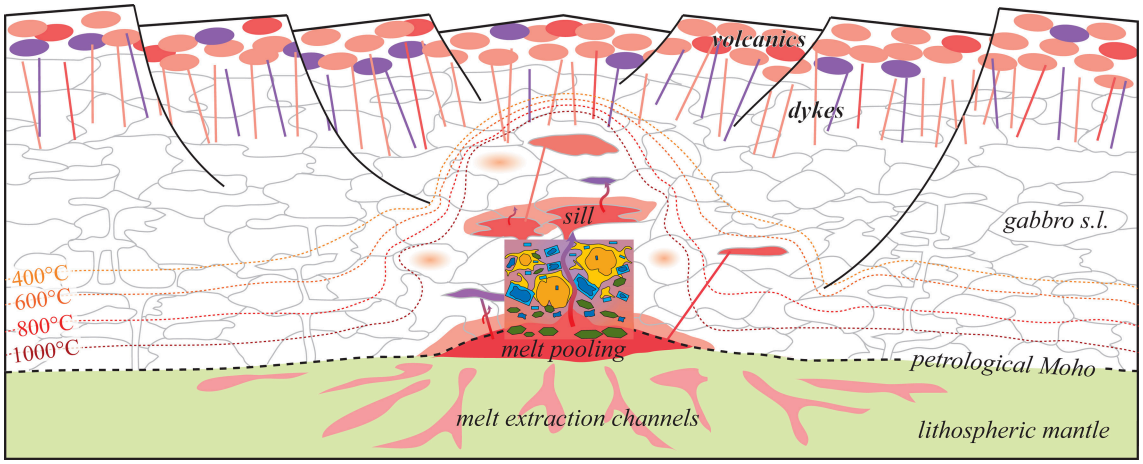

Graphical Abstract | Cross-section of slow-spreading ridges, showing the different occurrences of melt in the oceanic crust (based on Sinton and Detrick, 1992; Dick et al., 2008). Gabbro s.l. includes troctolite, olivine-gabbro, gabbro, gabbronorite and ferrogabbro. Also dunite occurs along the Moho. Young hot crustal gabbro reacts (i.e., partial melting, hybridization, recrystallization) with invading primitive mantle-derived melt. Crystals, rocks and melt chemistry and texture are modified.

INTRODUCTION

Mid-ocean ridge basalts (MORB) cover 60% of the Earth's surface area. Although MOR lavas do not evolve significantly and largely remain basaltic in composition, even primitive (as defined by Grove et al., 1992) high-MgO MORB magmas show a large scatter in major and trace elements and isotopic compositions (Shimizu, 1998). This variation has been attributed to (1) variable degrees of partial melting of the source (ca. 1,250–1,280°C) (Klein and Langmuir, 1987; Hirose and Kushiro, 1993; Kelemen et al., 1997a; Hirschmann et al., 1998); (2) variable mantle melting pressure (Klein and Langmuir, 1987; Hirose and Kushiro, 1993; Shimizu, 1998); (3) mantle source heterogeneity and metasomatism (e.g., lherzolite, harzburgite, pyroxenite) (Shimizu, 1998; Salters and Dick, 2002; Lambart et al., 2009); (4) mantle water content (Feig et al., 2006); (5) porous flow reaction between ascending melts and the ambient mantle (Quick, 1981; Collier and Kelemen, 2010) and lower crust (Coogan et al., 2000; Gao et al., 2007; Lissenberg et al., 2013; Coumans et al., 2016; Lissenberg and MacLeod, 2016); (6) mixing of primitive basalt with cotectic liquid (Dungan and Rhodes, 1978; Shorttle, 2015); (7) differentiation via fractional crystallization (Elthon, 1979; Quick, 1981; Grove et al., 1992; O'Neill and Jenner, 2012; Abily and Ceuleneer, 2013; Coogan and O'Hara, 2015).

Successive primitive magma batches (high-MgO basalt and possibly picrite; Elthon, 1979; Quick, 1981; Laubier et al., 2012), sourced from the partially molten asthenospheric mantle, are underplated along the Moho (Abily and Ceuleneer, 2013). Magma may subsequently intrude lower oceanic crustal plutons and crystal mushes (Sinton and Detrick, 1992) (**Graphical Abstract**). For slow-spreading ridges, Dick et al. (2008) showed that melt flow focuses to local magmatic centres and creates igneous complexes within the ridge segment. Their position varies in space and time rather than being fixed at a single central point, like may be the case with the axial melt lens in fast-spreading ridges (e.g., Coogan et al., 2002). Igneous complexes are thus built up incrementally, by accretion of successive sills or dykes (e.g., Dick et al., 2008; Allibon et al., 2011; Leuthold et al., 2014b).

Repeated intrusion of hot magma diffuses heat to the host rock, which may cause partial melting to various degrees (Bédard et al., 2000; Ridley et al., 2006; Holloway and Bussy, 2008; Solano et al., 2012; Leuthold et al., 2014a; Coumans et al., 2016). Assimilation of crustal partial melt in deep crustal hot zones (i.e., lower crust mafic sill complexes) can play a major role in magma differentiation (e.g., De Paolo, 1981; Hildreth and Moorbath, 1988; Solano et al., 2012). As a result, liquid and host rock/crystal mush chemistry and textures are modified, and new and secondary mineral phases crystallize from the hybrid melt (Eason and Sinton, 2009; Leuthold et al., 2014a, 2015). Melting and dissolution reactions are efficient and rapid (Donaldson, 1985; Tsuchiyama, 1986; Kvassnes and Grove, 2008), and have started to be recognized as an important MORB crustal

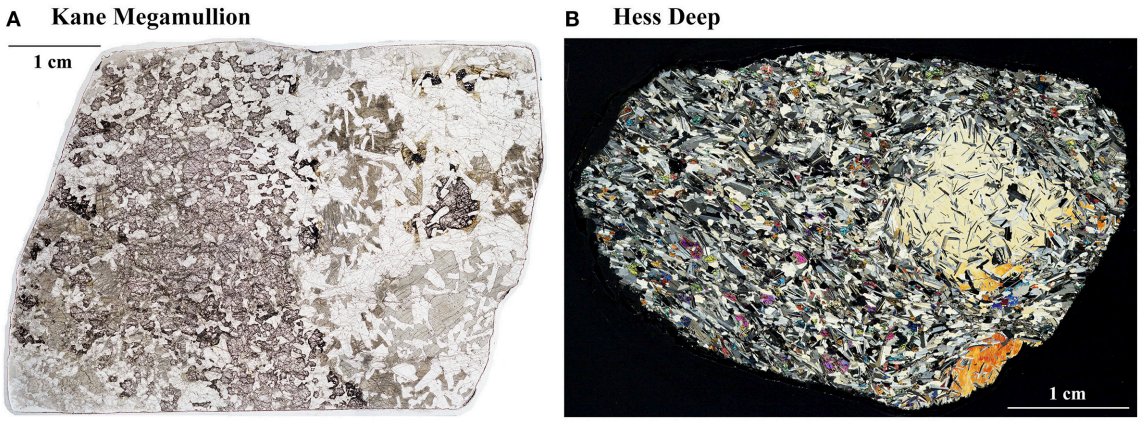

Figure 1 | (A) Kane Megamullion (23°30′N, Mid-Atlantic Ridge) JAS117-63 sample. From right to left, a coarse-grained poikilitic gabbro (with clinopyroxene oikocrysts) in contact with layers of fine-grained troctolite, grading to a medium-grained poikilitic gabbro (with interstitial clinopyroxene) and to a gabbro. See also **Figure A.1** and **Presentation 1**. **(B)** Hess Deep (2°15′N, 101°33′W, East Pacific Rise) U1415I_4R_2_9-13 lower oceanic crust sample (see Gillis et al., 2014b) with clinopyroxene oikocrysts in a foliated troctolitic groundmass. See also **Figure A.2**.

differentiation process through the oceanic crustal filter (Bédard et al., 2000), based on studies of oceanic glasses (O'Neill and Jenner, 2012), plutonic rocks (e.g., Coogan et al., 2000; Gao et al., 2007; Lissenberg and Dick, 2008; Lissenberg et al., 2013; Lissenberg and MacLeod, 2016), phenocryst melt inclusions (Laubier et al., 2012; Coumans et al., 2016), and plutonic xenoliths in MORB (Ridley et al., 2006). Similar observations are made in ophiolites (e.g., Bédard et al., 2000; Sanfilippo et al., 2015). Hence, lower oceanic crust partial melting can be an important differentiation process along mid ocean ridges. Identification and quantification of such partial melting processes contribute to our understanding of the thermal, chemical and thus rheological evolution of the young oceanic crust.

In an analog 2D study on the Rum layered intrusion (Scotland), Leuthold et al. (2014a) showed evidence for small scale partial melting of equigranular gabbro by invading hot picrite and formation of troctolitic restite, subsequently refertilized to poikilitic gabbro. In the present study, we have selected poikilitic gabbro samples from the slow-spreading Mid-Atlantic ridge, at Kane Megamullion, and from the fast-spreading Galapagos triple junction, at Hess Deep (**Figure 1**). We combine microtextural observations and mineral chemical measurements on clinopyroxene oikocrysts (oikocrysts are large crystals with several inclusions, named chadacrysts) to investigate high temperature partial melting of lower oceanic crust gabbro primocrysts (primocrysts are early formed crystals; i.e., at high temperature) by intrusion of primitive hot mantle-derived melts, and subsequent crystallization from hybrid melt. This early-stage Melting-Assimilation-Storage-Hybridization (MASH; Hildreth and Moorbath, 1988) process is distinct from the late-stage strong zoning and incompatible element fractionation commonly observed in clinopyroxene rims, resulting from reactive porous flow of interstitial differentiated melt with plagioclase ±olivine ±clinopyroxene (Coogan et al., 2000; Gao et al., 2007; Lissenberg et al., 2013; Lissenberg and MacLeod, 2016) or post-crystallization diffusive fractionation (Coogan and O'Hara, 2015).

The focus of this paper is threefold: (1) To identify gabbro partial melting and hybridization with mantle-derived melt by studying clinopyroxene oikocrysts cores; (2) To estimate the effect of gabbro assimilation on MORB chemistry; (3) To test whether lower oceanic gabbro partial melting is a thermally realistic process.

ANALYTICAL METHODS

Mineral element maps (**Figure 2**) were acquired using a five-spectrometer JEOL JXA-8200 electron microprobe analyser (EMPA) at ETH Zürich, with a 15 kV accelerating voltage and a beam current of 100 nA. Major element compositions of minerals were determined using a 15 kV accelerating voltage with a beam current of 20 nA. Natural and synthetic silicates and oxides were used as standards. Straight-line clinopyroxene core-rim profiles were not possible because of the occurrence of several plagioclase chadacrysts. Chemical maps and isolated measurements were used to reconstruct complete profiles.

Clinopyroxene and plagioclase trace element contents were analyzed *in situ* using a Thermo Element XR mass spectrometer at ETH Zürich, connected to a 193 nm Resonetics ArF Excimer laser. The laser was operated in a Laurin Technic S155 ablation cell with a spot size of 30 μm, a frequency of 5 Hz and a laser power density of 2 $J \cdot cm^{-2}$. The EMPA data were used as internal standards for all analyses. We used NIST SRM610 for external standardization and the GSD-1G basalt glass as a secondary standard. The raw data were reduced off-line using the SILLS software (Guillong et al., 2008). For 30 μm spots, 1σ uncertainties for REE and Sr are 4–7% (14% for La) and the deviation from certified values on secondary standard (GSD-1G) is <3–5% (except ca. 6–9% for Gd and Er). Core-rim profiles were

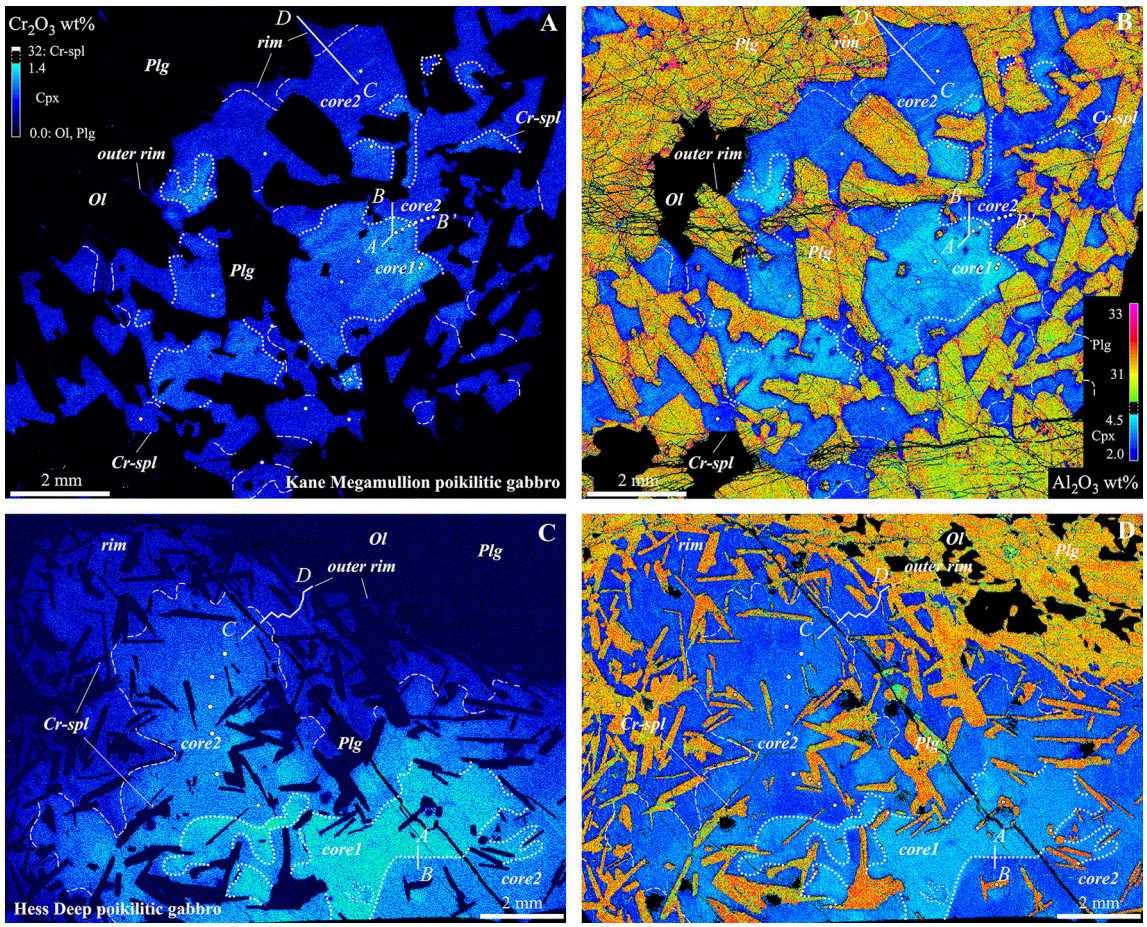

Figure 2 | Complex clinopyroxene microtextures revealed by EMPA X-ray Cr_2O_3 and Al_2O_3 maps. See also TiO_2 map in **Figure A.3**. **(A,B)** Kane Megamullion and **(C,D)** Hess Deep coarse-grained poikilitic gabbro in each case showing a clinopyroxene oikocryst in a clinopyroxene-free groundmass. In both samples, early formed core1 shows resorption texture and subsequent crystallization of chemically distinct clinopyroxene core2 and rim oikocrysts. Gray dots are isolated EMPA and LA-ICP-MS analyses, completing core1-core2 profile (A,B [B']) and core2-rim-outer rim profile (C,D).

duplicated with a reduced element list and spot sizes of 50 μm. For 50 μm spots, 1σ uncertainties for REE, Sr and Zr are 2–5% and the deviation from certified values on secondary standard (GSD-1G) is <5% (except ca. 8% for Gd).

RESULTS

Clinopyroxene core-rim profiles for selected elements are shown in **Figures 3**, **4**. More elements are plotted in **Tables A.1**, and **A.2**. Mg# (molar $Mg/[Mg + Fe^{2+} + Fe^{3+}]$) and Sr/Sr^* ($Sr_N/[(Pr_N + Nd_N)/2]$) (1σ ≈ 6%, error ≈ 0.5%) variations across clinopyroxene oikocryst core-rim transects are not as sharply-defined as for slow-diffusing tri- and tetravalent cations (Ti, Al, Cr, REE), presumably because of faster diffusion. $Sr/Sr^* < 1$ (i.e., negative Sr anomaly) is commonly interpreted as a consequence of plagioclase fractionation (e.g., Leuthold et al., 2014b). Analyses close to intra-crystal cracks frequently show strong decreases in Mg# (**Table A.2**), and were discarded. The clinopyroxene and plagioclase Fe^{3+}/Fe_{tot} ratio was estimated based on the mineral stoichiometry.

Mid-Atlantic Ridge Poikilitic Gabbro

The Kane Megamullion (Mid-Atlantic Ridge, 23°30′N) is an oceanic core complex comprising a series of domes oriented parallel to the spreading direction (Dick et al., 2008). The average spreading rate is 14.4 mm/year to the west and 9 mm/year to the east (Williams, 2007). The plutonic suite was sampled by the Jason ROV during the R/V Knorr cruise 180-2 in the Fall of 2004. It is composed of troctolite (14.9% of all collected gabbro s.l. samples by number), olivine gabbro (34.1%), ferrogabbro (i.e., oxide gabbro) (26.9%) and metagabbros (24.1%) (Dick et al., 2008). We have studied a coarse-grained poikilitic gabbro (JAS117-63), crystallized under lower oceanic crustal conditions. This sample was previously described by Lissenberg and Dick (2008) who reported details of several poikilitic gabbros through the oceanic crustal section.

This sample shows alternating layers (1–5 cm wide) of a coarse-grained poikilitic gabbro in contact with a fine-grained troctolite grading to a medium-grained gabbro with interstitial clinopyroxene (i.e., referred to as medium-grained poikilitic gabbro in this study) to a gabbro (**Figure 1A**). This study mainly

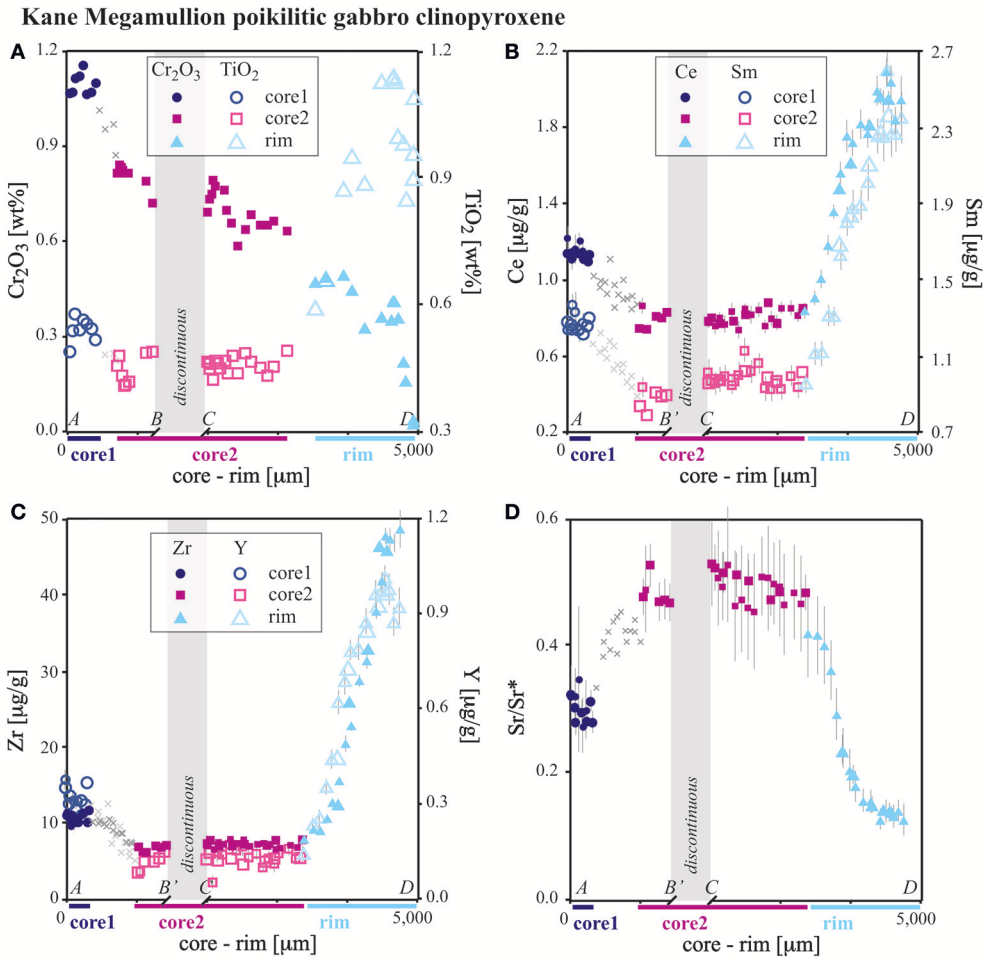

Figure 3 | Chemical variations across a zoned clinopyroxene in Hess Deep lower oceanic crust poikilitic gabbro: **(A)** Cr_2O_3 and TiO_2, **(B)** Ce and Sm, **(C)** Zr and Y and **(D)** Sr/Sr*. See profile locations in **Figures 2A,B** ($core1_{KM}$-$core2_{KM}$: A,B [B'], $core2_{KM}$-rim_{KM}-outer rim_{KM}: C,D). Overgrown $core2_{KM}$ is depleted in compatible Cr_2O_3, moderately incompatible TiO_2, HREE (e.g., Sm) and Y and strongly incompatible LREE (e.g., Ce) and Zr. $Core2_{KM}$ shows higher Sr/Sr* ratio than in anhedral $core1_{KM}$ (see other elements in **Table A.1**). The associated dissolution texture and chemical zoning are best explained by assimilation of a gabbroic assemblage and recrystallization from basalt-gabbro hybrid melt. Late-stage outer rim_{KM} shows strong TiO_2, REE, Y and Zr increases and Cr_2O_3, Sr/Sr* (and Mg#) decreases. Gray crosses are non-plateau analyses, partly reequilibrated upon diffusion. Large symbols are LA-ICP-MS 51 µm spot analyses. 1σ error bars are shown for trace elements. Data in **Table A.1**.

focuses on the coarse-grained poikilitic gabbro, with ca. 0.5–2 cm clinopyroxene oikocrysts. Detailed X-ray EMPA mapping of clinopyroxene oikocrysts in the coarse-grained poikilitic gabbro (**Figures 2A,B**, **Figure A.3A**), along with EMPA and laser ablation ICP-MS major and trace element data (**Figures 3**, **5**, **6A**, **Table A.1**), show complex Cr, Ti, REE, Zr and Y (and also partly re-equilibrated Fe and Mg) zoning along sharp contacts between successive clinopyroxene generations: $core1_{KM}$ (subscript KM and HD are used to distinguish between Kane Megamullion and Hess Deep clinopyroxene generations), $core2_{KM}$ and the rim_{KM}. $Core1_{KM}$ is anhedral with few small plagioclase chadacrysts. It is overgrown by poikilitic $core2_{KM}$, which is in turn overgrown by the poikilitic rim_{KM} (**Figure 2**). $Core1_{KM}$ is Cr- and Al-rich and moderately Ti-, Zr- and REE-rich (Mg#: 86.8, Cr_2O_3: 1.1 wt.%, Sm: 1.26 µg/g, ∑REE: 15.83 µg/g, Zr: 11.63 µg/g, Sr/Sr* = 0.29). $Core2_{KM}$ is Mg-rich, moderately Cr- and Al-rich and Zr- and REE-poor and shows discrete zoning (Mg#: 88.0, Cr_2O_3: 0.84 to 0.63 wt.%, Sm: 0.84 to 1.01 µg/g, ∑REE: 12.06 µg/g, Zr: 6.2 to 7.7 µg/g, Sr/Sr* = 0.48). Cr_2O_3, Al_2O_3 and Mg# progressively decrease and TiO_2, Zr and REE progressively increase (Mg#: 86.7 to 85.1, Cr_2O_3: 0.50 to ca. 0.03 wt.%, Sm: 1.21 to 2.30 µg/g, ∑REE: 13.96 to 26.52 µg/g, Zr: 9.19 to 45.36 µg/g, Sr/Sr* = 0.35 to 0.14) toward the oikocryst outermost rim_{KM}. In the adjacent troctolite to medium-grained poikilitic gabbro to gabbro layer, the clinopyroxene cores have similar major and trace element compositions as the coarse-grained poikilitic gabbro outer $core2_{KM}$, while interstitial clinopyroxene has higher Cr_2O_3 concentrations (**Table A.1**).

The clinopyroxene oikocrystic $rims_{KM}$ enclose reversely-zoned anhedral to euhedral plagioclase chadacrysts (An_{71-68} cores to An_{82-69} rims). No olivine chadacrysts are observed. Cr-spinel crystals (ca. 5 µm) occur along plagioclase-clinopyroxene

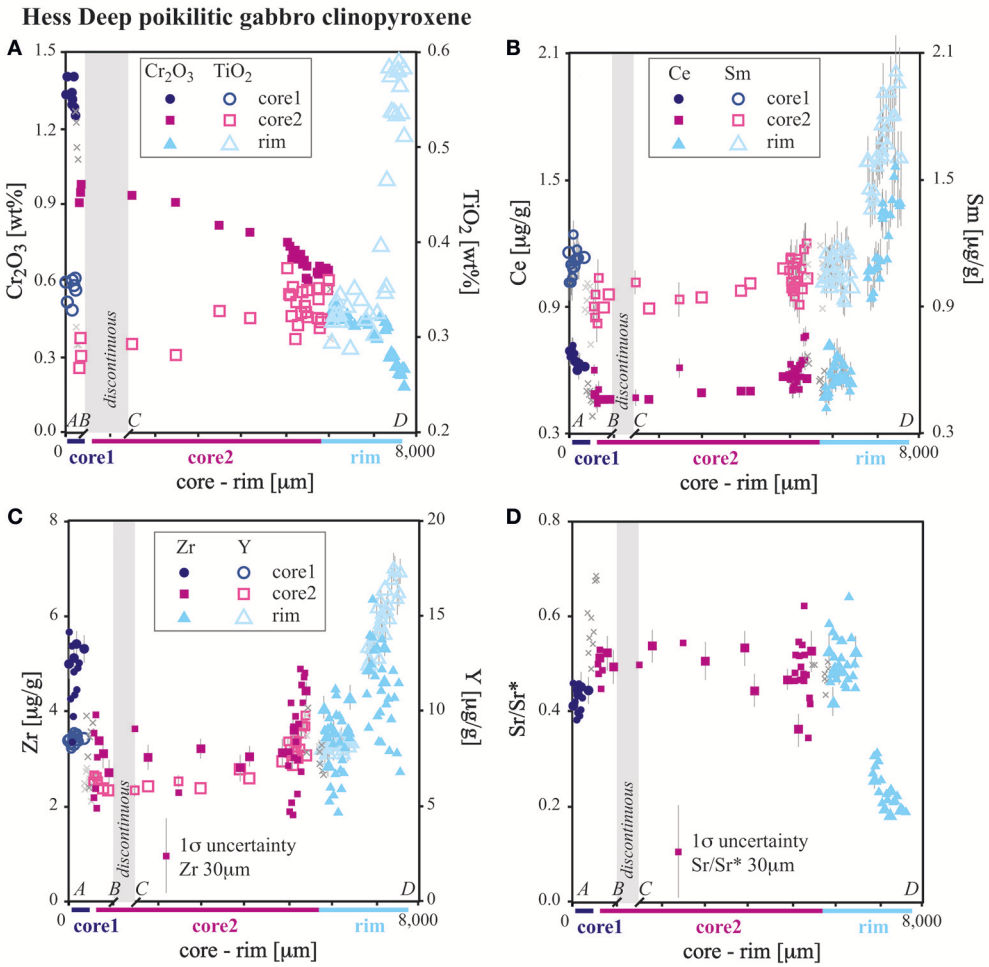

Figure 4 | Chemical variations across a zoned clinopyroxene in Hess Deep lower oceanic crust poikilitic gabbro: **(A)** Cr_2O_3 and TiO_2, **(B)** Ce and Sm, **(C)** Zr and Y and **(D)** Sr/Sr*. See profile locations in **Figures 2C,D** ($core1_{HD}$-$core2_{HD}$: A,B, $core2_{HD}$-rim_{HD}-outer rim_{HD}: C,D). Geochemical profiles are very similar to those from the Kane Megamullion clinopyroxene oikocryst (see **Figure 3**). Gray crosses are non-plateau analyses, partly reequilibrated upon diffusion. Large symbols are LA-ICP-MS 51 µm spot analyses. 1σ error bars are shown for trace elements. Data in **Table A.2**.

grain boundaries (**Figure 2A**). The poikilitic gabbro groundmass is composed of coarse-grained (ca. 3 mm) reversely-zoned subhedral plagioclase (An_{71-68} core to An_{81-79} rim) (**Figures 2B**, **7A**) and anhedral olivine (Fo_{84-83}). In the troctolite layer, plagioclase crystals show normal zoning from An_{83-81} to An_{81-72} (**Figure 7A**, **Table A.1**) and olivine crystals have Fo_{85} contents (see Lissenberg and Dick, 2008, for details). In the medium-grained poikilitic gabbro and gabbro layers, the plagioclase crystals show similar normal zoning (An_{81} core to An_{79-71} rim) as in the adjacent troctolite layer (**Table A.1**). The plagioclase Sr concentration varies between 190 and 250 µg/g, being relatively homogeneous in the poikilitic gabbro and troctolite layers. The Sr/Sr* is higher in poikilitic gabbro plagioclase chadacrysts (70-30) and in troctolite plagioclase (50-40; one An_{81} plagioclase with a value at 70) than in the poikilitic gabbro groundmass (40-20, with one An_{75} plagioclase chadacryst in olivine with Sr/Sr* = 60) (**Figure 7A**).

East Pacific Rise Poikilitic Gabbro

Fast-spreading ridge (ca. 65 mm/year) lower oceanic crust is exposed at Hess Deep (Francheteau et al., 1990), which is located close to the Galapagos triple junction between the East Pacific Rise and the Galapagos rift (2°15′N, 101°33′W). The plutonic suite is mostly composed of (impregnated) dunite, layered troctolite, olivine gabbro and gabbro in the lower part of the section and oxide-bearing gabbronorite in the upper ca. 1,800 m (Lissenberg et al., 2013; Gillis et al., 2014a). Layering is considered to have formed whilst the rocks were still at a crystal mushy state (Gillis et al., 2014a). We present data here for poikilitic gabbro 345_U1415I-4R_2_9-13 (**Figure 1B**), drilled during IODP Expedition 345 from the deeper part of the section. Clinopyroxene-oikocryst bearing troctolites and gabbros are common in the Hess Deep lower crust (Lissenberg et al., 2013; Gillis et al., 2014a).

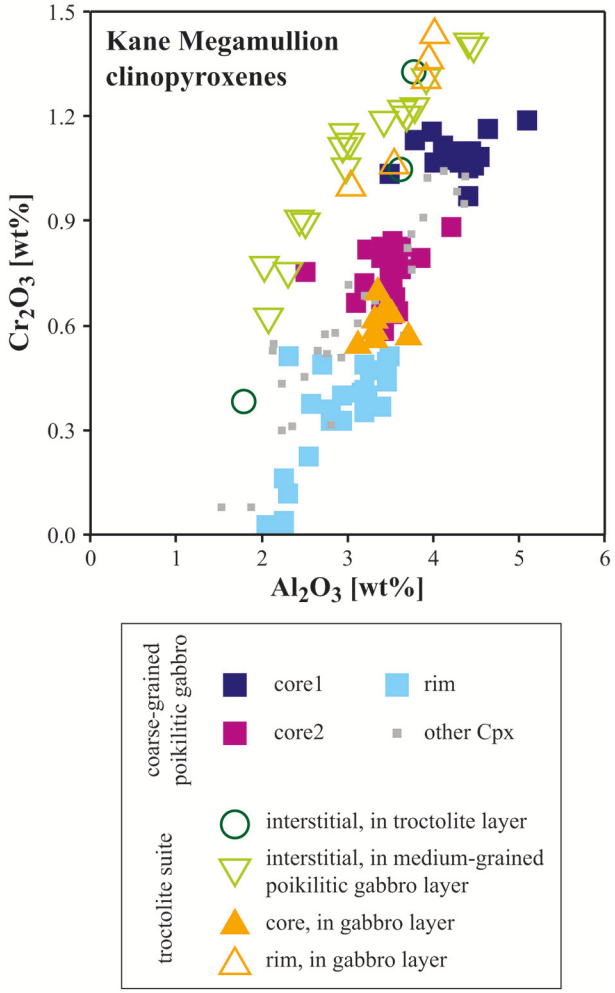

Figure 5 | Chemistry of Kane Megamullion clinopyroxene grains in the coarse-grained poikilitic gabbro and the troctolite, medium-grained poikilitic gabbro and gabbro layers.

Clinopyroxene oikocryst (ca. 1 cm diameter) X-ray maps (**Figures 2C,D**, **Figure A.3B**) and geochemical core-rim profiles show complex textures and zoning (**Figures 4**, **6B**, **Table A.2**). Anhedral core1$_{HD}$ shows resorption embayments. It is overgrown by poikilitic core2$_{HD}$, which is in turn overgrown by the poikilitic rim$_{HD}$ to the outermost interstitial rim$_{HD}$ (**Figures 2C,D**). Core1$_{HD}$ is Cr-, Al-rich, moderately Ti-, Zr- and REE-rich (Mg#: 88.4, Cr_2O_3: 1.3 wt.%, Sm: 0.71 µg/g, ∑REE: 8.84 µg/g, Zr: 4.64 µg/g, Sr/Sr* = 0.41). Slow-diffusing Cr_2O_3 shows a sharp contact against overgrown core2$_{HD}$. Core2$_{HD}$ is moderately Cr- and Al-rich and Zr- and REE-poor and shows discrete normal zoning (Mg#: 88.4 to 87.5, Cr_2O_3: 0.94 to 0.65 wt.%, Sm: 0.52 to 0.61 µg/g, ∑REE: 6.70 to 8.86 µg/g, Zr: 2.75 to 3.90 µg/g, Sr/Sr* = 0.51 to 0.49) (**Figure 4**). Sr/Sr* increases to 0.68 at the transition between core1$_{HD}$ and core2$_{HD}$. The decrease in Cr_2O_3, Al_2O_3 and Mg# and increase in TiO_2, Zr and REE is more marked in the rim$_{HD}$ toward the outer rim$_{HD}$ (Mg#: 87.6 to 83.4, with a final increase to 85.7, Cr_2O_3: 0.48 to 0.19 wt.%, Sm: 0.63 to 1.25 µg/g, ∑REE: 8.19 to 15.68 µg/g, Zr: 3.37 to 4.33 µg/g, Sr/Sr* = 0.51 to 0.20). The TiO_2 content of the clinopyroxene oikocryst increases close to plagioclase chadacrysts (**Figure A.3B**). Plagioclase chadacrysts are small and randomly oriented in the clinopyroxene core1$_{HD}$ and are larger and sub-parallel to the groundmass foliation in the rim$_{HD}$. Plagioclase compositions in core1$_{HD}$ are An_{82-81} and An_{81-78} in core2$_{HD}$ and rim$_{HD}$ (**Figure 7B**, **Table A.2**). Olivine chadacrysts are not observed. Fine-grained Cr-spinel grains occur along clinopyroxene core1$_{HD}$ -core2$_{HD}$ and core2$_{HD}$ -rim$_{HD}$ contacts, in close spatial association with plagioclase. The well-defined foliation in the groundmass appears to wrap around clinopyroxene oikocrysts (see Gillis et al., 2014b). The groundmass is composed of fine-grained (ca. 1 mm) subhedral plagioclase (with discrete reverse zoning from An_{78-75} core to An_{80-76} rim) and anhedral olivine (Fo_{81}). Lissenberg et al. (2013) showed dissolution fronts in plagioclase (their **Figure 6**), with strong and sharp core-rim zoning ($An_{\sim75}$ to $An_{\sim35}$). The plagioclase Sr concentration varies from 140 to 320 µg/g. Sr/Sr* decreases from the plagioclase chadacrysts in clinopyroxene core1$_{HD}$ (60–80) to those in core2$_{HD}$ and rim$_{HD}$ (30–50) (**Figure 4D**). The groundmass plagioclase crystals have relatively homogeneous (low) Sr/Sr* of 20–30.

DISCUSSION

In the following discussion, we first use experimental petrology and MELTS (Ghiorso and Sack, 1995) calculations to determine the liquid line of descent of primitive mantle-derived melts and the associated cumulate composition and chemistry. We then use partition coefficients to calculate parental melts in equilibrium with core1 and core2 clinopyroxene. Using mineral textures and zoning, we discuss the core1 to core2 geochemical evolution with respect to equilibrium and fractional crystallization and to the MASH model of Hildreth and Moorbath (1988). We then explore the importance of lower oceanic crust partial melting undergoing intrusion by hot mantle-derived melt, using thermal modeling. Finally, we discuss the effects of gabbro partial melting and assimilation on the composition and chemistry of MOR lavas and the lower oceanic crust.

MOR Melts Liquid Line of Descent and Primitive Gabbro Cumulates

Mantle-Derived Melt Liquid Line of Descent

The mantle source partial melting conditions strongly determine the derivative melt composition (e.g., Klein and Langmuir, 1987; Hirose and Kushiro, 1993; Kelemen et al., 1997a; Hirschmann et al., 1998). Deep melting produces Mg-rich and Si-, Al-poor primitive melt and high degree partial melting generates Mg-, Cr-rich and Al-poor melt (**Figure 8**).

We have employed the MELTS algorithm (Ghiorso and Sack, 1995) to calculate the liquid and solid lines of descent of mantle-derived melt at crustal pressures. We have considered an averaged primitive glass composition (MgO>9.5, Mg#>62, 49>SiO_2 >47.5 wt.%) from the Mid-Atlantic Ridge (23 to 37°N) databases of Gale et al. (2013) and PetDB (Lehnert et al., 2000)

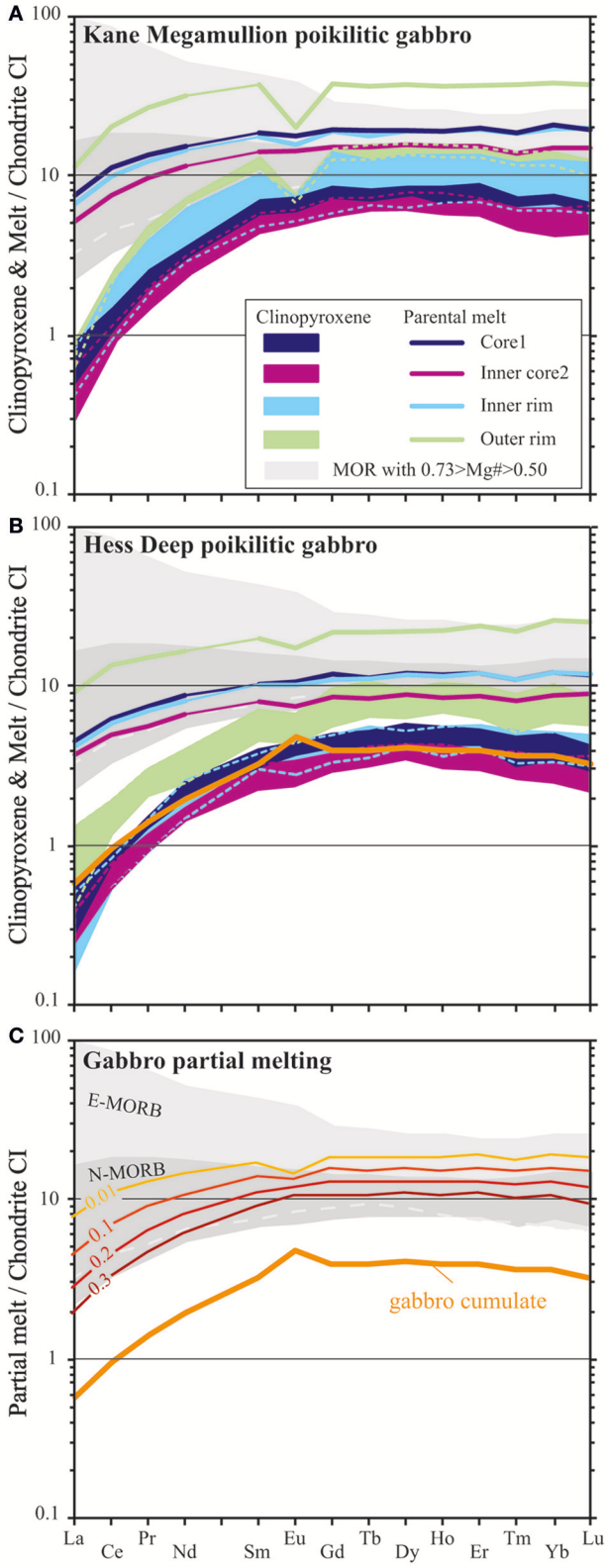

Figure 6 | Chondrite CI- (Boynton, 1984) normalized clinopyroxene core1, inner core2 (only inner part in Hess Deep), rim and outer rim REE compositions *(Continued)*

Figure 6 | for **(A)** Kane Megamullion and **(B)** Hess Deep poikilitic gabbros. Inner core2 is REE-depleted in comparison to core1 (and REE concentration gradually increases toward outer core2$_{HD}$ in Hess Deep) (see **Figures 3**, **4**). Clinopyroxene chemistry is comparable to lower oceanic crust clinopyroxene (e.g., Kelemen et al., 1997b). Equilibrium melts were calculated using Wood and Blundy (1997) partition coefficients. MORB glass chemistry from Gale et al. (2013) and PetDB (Lehnert et al., 2000) databases. **(C)** Composition of a lower oceanic crust gabbro cumulate, estimated using the crystal cores chemistry and modal assemblages calculated with MELTS (Ghiorso and Sack, 1995). The partial melt composition (at liquid fraction $F = 1$, 10, 20, and 30%) was calculated using modal fractional melting equation (see **Table A.3**).

(see **Table A.3**). We have run liquid lines of descent from 50 MPa to 200 MPa, from dry to 0.5 wt.% H_2O (natural MORB have ca. 0.1–0.6 wt.% H_2O, with an average of 0.2 wt.% H_2O; Clog et al., 2013, and references therein), at NNO to NNO-2 (Righter et al., 2006) and assuming either equilibrium or fractional crystallization. Results are shown in **Figure 8** and discussed hereafter.

Experimental petrology (e.g., Tormey et al., 1987; Grove et al., 1992) and MELTS (Ghiorso and Sack, 1995) calculations on primitive mantle-derived melt at crustal pressures successively crystallize olivine on the liquidus, followed by plagioclase shortly followed by clinopyroxene, and finally low-Ca clinopyroxene, pigeonite and orthopyroxene. The cumulates formed in the models are Cr-spinel bearing dunite, troctolite, gabbro and gabbronorite, assuming crystallization with a strong component of fractionation. At 150 MPa, 0.2 wt.% H_2O and an initial Fe^{3+}/Fe_{tot} ratio corresponding to NNO-1 (≈NNO-2 at 1050°C) conditions, olivine saturates at ca. 1,225°C, plagioclase at ca. 1,220°C and clinopyroxene at ca. 1,205°C. Plagioclase, olivine and mostly clinopyroxene saturation temperatures gradually increase with increasing pressure. Plagioclase stability strongly decreases at higher water content. Since plagioclase and clinopyroxene co-crystallize, the liquid fraction decreases significantly (i.e., up to ca. 2 vol.%/°C, from ca. 90 vol.%). Low Ca-pyroxene (fractional and equilibrium crystallization) and/or orthopyroxene (equilibrium crystallization) saturate last, replacing olivine at temperatures <1,150°C and <1,055°C, respectively. Low-Ca clinopyroxene, pigeonite and orthopyroxene were not observed in the two studied samples and we did not observe any evidence that either existed at an earlier stage. However, orthopyroxene occurs as a minor cumulus phase in Hess Deep primitive layered gabbro (in the same drill site 345-U1415I-4R; sometimes occurring as isolated crystals in olivine-gabbro or in orthopyroxene-rich bands; Gillis et al., 2014a,b). Orthopyroxene also occurs as oikocrysts and as exsolution lamellae in clinopyroxene cores in Hess Deep high-level gabbroic cumulates (Natland and Dick, 1996).

Our MELTS (Ghiorso and Sack, 1995) calculations are comparable to the Mid Atlantic Ridge, East Pacific Rise and Galapagos rift MORB glass database of Gale et al. (2013) and PetDB (Lehnert et al., 2000), in the area of the studied samples. A selection of major elements is presented in **Figure 8**. The MELTS algorithm gives reasonable estimates of the melt, olivine and clinopyroxene Mg# (Leuthold et al., 2015), and the lower oceanic crust primitive gabbro bulk rock Mg# composition (Gillis et al.,

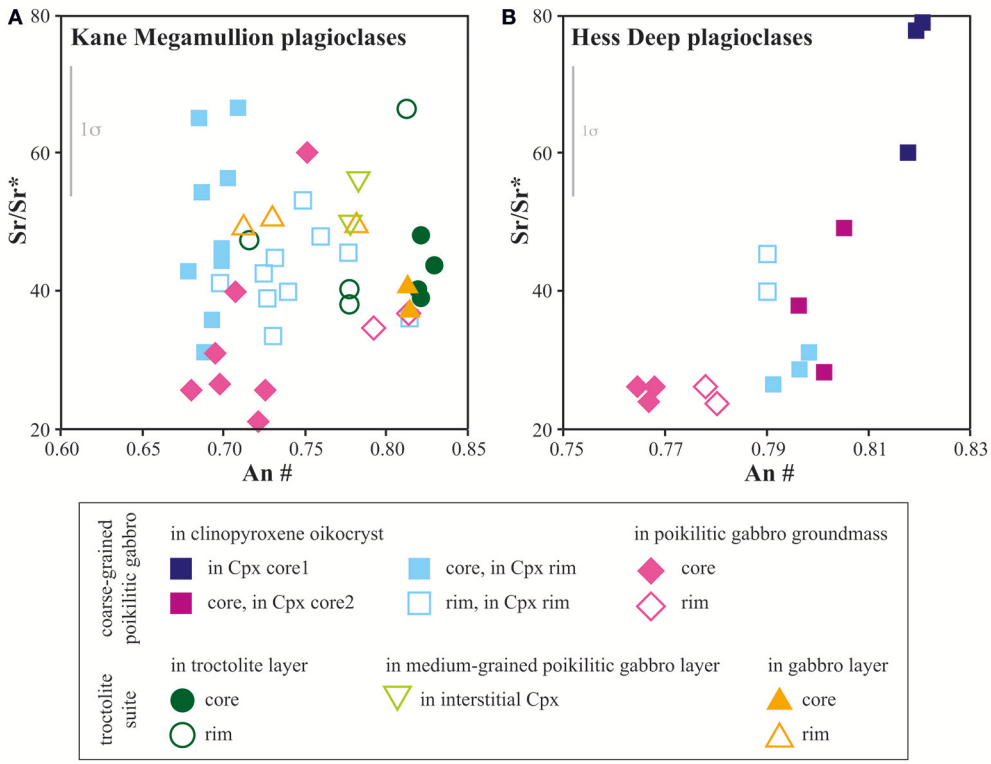

Figure 7 | Plagioclase Sr/Sr* vs. An composition in **(A)** Kane Megamullion poikilitic gabbro clinopyroxene and groundmass, and in troctolite, medium-grained poikilitic gabbro and gabbro layers and in **(B)** Hess Deep poikilitic gabbro clinopyroxene and groundmass. The anorthite content shows reverse zoning in poikilitic gabbros and normal zoning in troctolite, medium-grained poikilitic gabbro and gabbro layers. The groundmass Sr/Sr* is low.

2014a) overlaps with our gabbro cumulate MELTS calculations (**Figure 8**). The MELTS calculations and geochemical results appear identical at 150 MPa, at least until saturation of Fe-Ti oxides (ca. 1,100°C). Upon gabbro fractionation, the liquid is progressively depleted in MgO, Mg#, Al_2O_3, Cr_2O_3 and CaO. The melt SiO_2 concentration is nearly constant during crystallization of clinopyroxene and slightly decreases after the peritectic reaction of olivine to pigeonite or orthopyroxene. The melt SiO_2 strongly increases at constant Mg# with magnetite crystallization, which strongly depends on the magma redox condition. The selected starting composition is SiO_2-poor (<49 wt%) in comparison to other high Mg# MORB, likely produced at lower pressure. The liquid line of descent of such a SiO_2-rich MOR melt (SiO_2 >50 wt%, Mg#>60) and generated cumulates is comparable to the ones described here.

Origin of Clinopyroxene Core1 Primocrysts

The use of MELTS (Ghiorso and Sack, 1995) clinopyroxene chemistry to estimate the clinopyroxene core1 crystallization conditions is difficult, as CaO shows no zoning, Fe and Mg were partly reequilibrated and Cr in clinopyroxene is not considered in MELTS. MELTS predicts clinopyroxene strong TiO_2 enrichment upon crystallization, from 0.3 at 1,205°C to 1.3 wt% at 1,100°C, independent of equilibrium or fractional crystallization from parental Si-poor or Si-rich MOR melt. With low TiO_2 concentrations, Kane Megamullion clinopyroxene $core1_{KM}$ (0.55 wt%) and Hess Deep clinopyroxene $core1_{HD}$ (0.35 wt%) probably crystallized at high temperatures of ca. 1,160°C and ca. 1,200°C, respectively. MELTS also predicts a decrease in the plagioclase anorthite content upon fractional crystallization, from An_{81} at 1,220°C to An_{43} at 1,000°C. Plagioclase chadacrysts in Hess Deep (An_{82-81}) clinopyroxene core 1 crystallized at ca. 1,220°C. The crystallization temperature estimates for clinopyroxene and plagioclase are in agreement. The clinopyroxene $core1_{KM}$ and $core1_{HD}$ crystallized after moderate (1,160°C corresponds to ~50% crystallization) to low (1,200°C corresponds to ~25% crystallization) crystal fractionation, respectively, from primitive mantle-derived melt.

Cr_2O_3, TiO_2 and the REE are relatively immobile elements whose concentration evolves quickly upon crystallization. Thus, they represent ideal elements to calculate clinopyroxene parental magma chemistry, using partition coefficients. Based on high MgO-basalt and basalt equilibrium and fractional crystallization experiments at one atmosphere and 200, 700, and 800 MPa (Grove and Bryan, 1983; Grove et al., 1992; Villiger et al., 2007; Bédard, 2014; Leuthold et al., 2015), the clinopyroxene-melt partition coefficient for Cr_2O_3 decreases upon cooling from ca. 20 [at oxygen fugacity <NNO, typical for MOR lavas (Righter et al., 2006)] to ca. 3. The partition coefficient for TiO_2 is constant at 0.6–0.2. The Kane Megamullion clinopyroxene $core1_{KM}$ (1.1 wt% Cr_2O_3, 0.52 wt% TiO_2) and Hess Deep clinopyroxene $core1_{HD}$ (1.3 wt% Cr_2O_3, 0.36 wt%

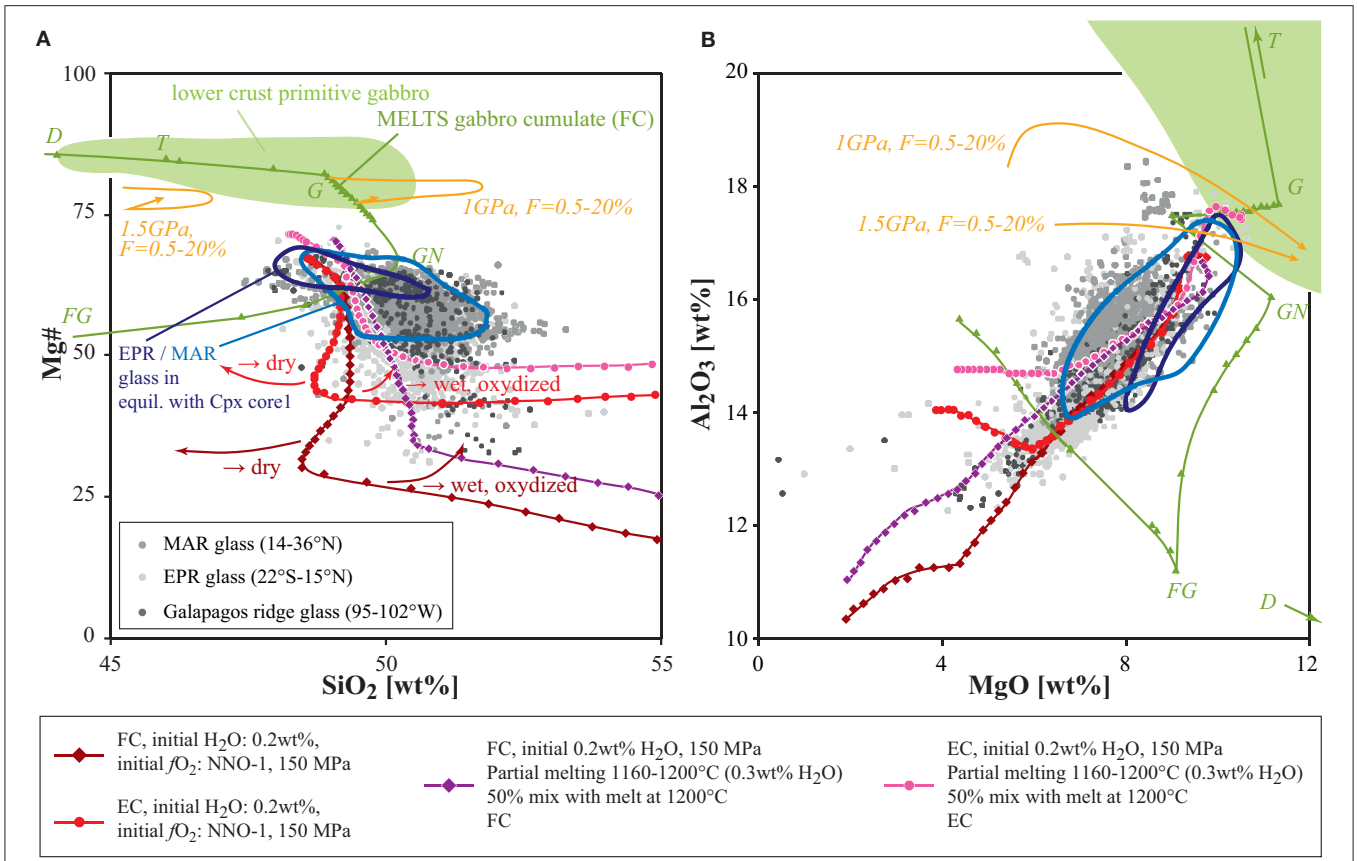

Figure 8 | Effect of gabbro cumulate assimilation on mantle-derived melt chemistry, with **(A)** Mg# vs SiO_2 and **(B)** Al_2O_3 vs MgO. MORB glass [database from Gale et al. (2013), and PetDB, (Lehnert et al., 2000)] sampled along Mid Atlantic Ridge, East Pacific Rise and Galapagos rift axes, close to Kane Megamullion and Hess Deep, are shown. Spinel lherzolite partial melting arrows show the chemical evolution of mantle-derived melt upon pressure (1 to 1.5 GPa) and partial melting ($F = 0.5$ to 20%) increases [pMELTS by Ghiorso et al. (2002); based on KLB-1 spinel lherzolite of Hirose and Kushiro (1993), see composition in **Table A.3**] [note: partial melting of olivine-poor lherzolite produces a melt with lower Mg#, as seen in experiments by Hirose and Kushiro (1993)]. The dunite (*D*), troctolite (*T*), gabbro (*G*), gabbronorite (*GN*) and ferrogabbro (*FG*) cumulates calculated using MELTS [fractional crystallization of primitive MOR glass (see **Table A.3**) at NNO-1, 0.2 wt.% H_2O and 0.15 GPa] reproduces the lower oceanic crust gabbro primitive cumulate from Gillis et al. (2014a). The melt liquid lines of descent, assuming pure fractional crystallization (FC) and equilibrium crystallization (EC), show early MgO and Al_2O_3 decreases and subsequent SiO_2 increase due to magnetite crystallization. At higher water content and/or oxygen fugacity, the melt becomes SiO_2-rich at high Mg#. Gabbro partial melting and hybridization with hot mantle-derived melt results in little but distinct physical and chemical modifications of the percolating primitive MOR melts [but may be confused with other parameters (e.g., water content, oxygen fugacity, pressure, equilibrium vs. fractional crystallization)]. The clinopyroxene core1 parental magma chemistry was determined using the major element chemistry of glass sampled close to Kane Megamullion and Hess Deep and whose TiO_2, Cr_2O_3, and REE (Ce/Sm and Sm on **Figure 9**) are equivalent to the calculated core1 parental magma (see text for discussion of the partition coefficients).

TiO_2) primocrysts likely crystallized from a basalt with high Cr_2O_3 (ca. 0.06–0.11 wt%) and low TiO_2 (0.6 to 2.6 wt%). Assuming a plagioclase-basalt TiO_2 partitioning of 0.048 (D_{TiO2} at 1200°C, Thy et al., 2006) for the Hess Deep poikilitic gabbro plagioclase chadacrysts (0.04–0.07 wt% TiO_2) in $core1_{HD}$, the parental magma TiO_2 concentration is 0.9–1.6 wt%. This corresponds to calculations based on the clinopyroxene $core1_{HD}$. Natural basaltic glasses with such compositions are MgO-rich (> 8.4 wt%) (see Gale et al., 2013, and the PetDB (Lehnert et al., 2000 databases). In the Hirose and Kushiro (1993) partial melting experiments of the relatively fertile KLB-1 spinel-lherzolite at 1.5 GPa, the solidus temperature is ca. 1,280°C [confirmed by pMELTS, (Ghiorso et al., 2002) calculations]. Upon increased degree of partial melting, the melt Cr_2O_3 concentration increases (up to 0.36 wt%). Melting of a mantle pyroxenite component also produces a Cr-rich melt (Lambart et al., 2009).

The clinopyroxene core1 compositions presented in this study have similar major element characteristics as Cr-, Mg-and Ti-rich clinopyroxene analyzed by Miller et al. (2009) in the Mid-Atlantic Ridge Atlantis Massif (in troctolite and olivine gabbro). Lissenberg and MacLeod (2016) interpreted such Cr-rich clinopyroxene as a product of basalt reaction with troctolite spinel. We suggest here that Cr-rich clinopyroxene may have crystallized from primitive MOR melt.

The parental magma REE composition for clinopyroxene core1 was calculated using the partition coefficient predictive model of Wood and Blundy (1997). The REE partitioning depends on the crystal chemistry, itself buffered by the change in temperature and melt Mg# from core1 to core2 to rim and outer

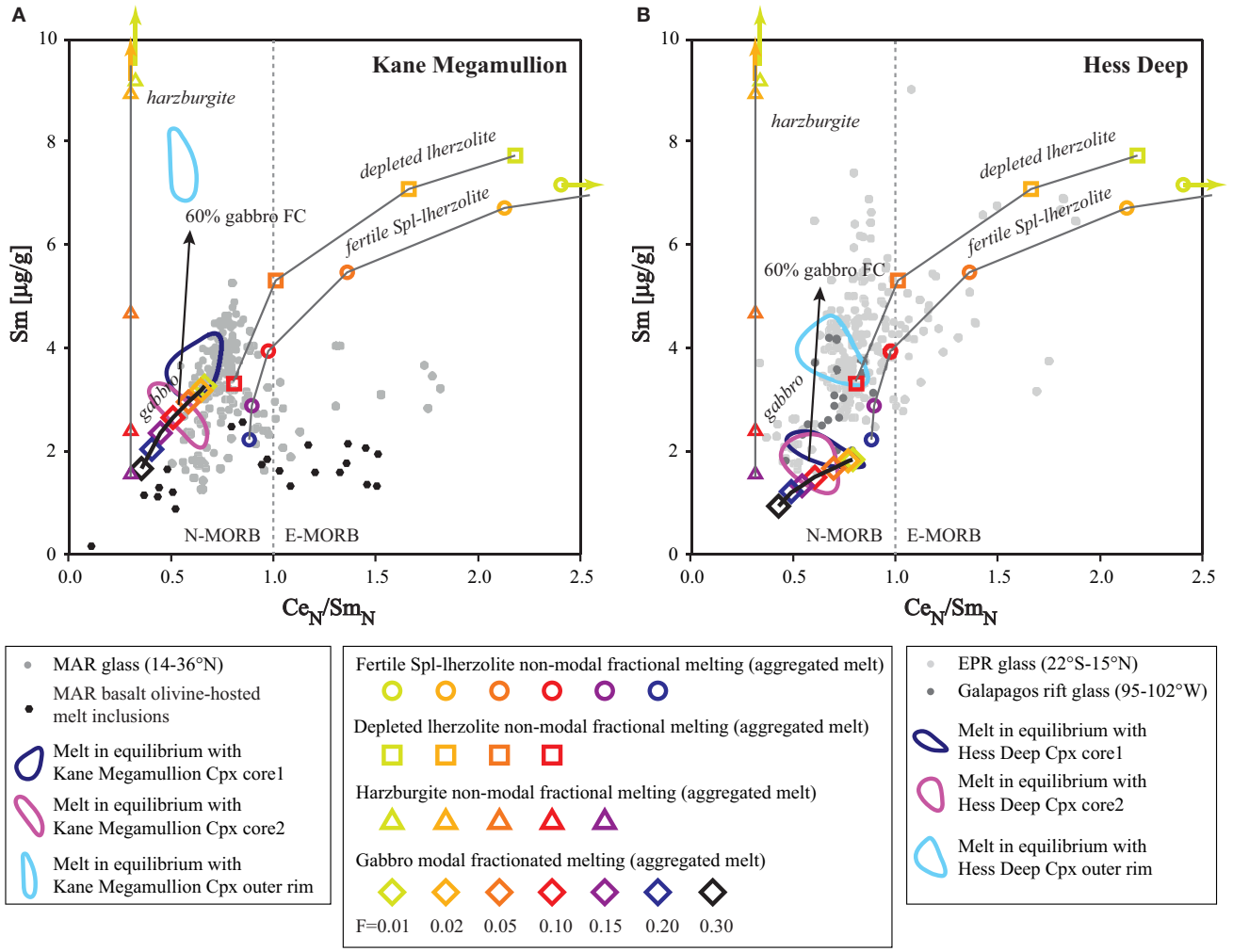

Figure 9 | Geochemistry of natural **(A)** Mid Atlantic Ridge (MAR) and **(B)** East Pacific Rise (EPR) and Galapagos rift glasses, sampled close to Kane Megamullion and Hess Deep [(Gale et al., 2013), and PetDB, (Lehnert et al., 2000) databases]. Mid-Atlantic Ridge basalt (36°N, 9°N) high-Mg olivine-hosted melt inclusions are shown for comparison (some of which contain too much clinopyroxene components) (Sobolev and Shimizu, 1993; Shimizu, 1998). The Kane Megamullion and Hess Deep clinopyroxene core1 are in chemical equilibrium with the basaltic glass having low Sm concentration and low Ce/Sm ratio. Such compositions can be reproduced by depleted spinel-lherzolite to harzburgite partial melting (liquid fraction F ≈ 0.05–0.15) (starting compositions by Jochum et al., 1989) (modal and non-modal and also equilibrium and Rayleigh fractional melting with aggregated melts give very similar results). The melt chemistry in equilibrium with the clinopyroxene core2 is Sm-depleted and has low Ce/Sm in comparison to core1. In combination with resorption textures (**Figure 2**) and complex zoning (**Figures 3**, **4**), it seems likely that hybridization of lherzolite-derived melt (F = 10–20%) with gabbro partial melts (F = 10–30%) in variable proportions occurred. The MOR melt samples with such chemical characteristics may have been overprinted by gabbro assimilation during transport through and storage in the lower oceanic crust. Upon gabbro fractional crystallization (FC), the melt Sm concentration increases at nearly constant Ce/Sm ratio. See **Table A.4** for geochemical modeling of partial melting.

rim, and thus remains nearly unchanged upon differentiation. Our resulting estimates match previously reported compositions for the Mid Atlantic Ridge, East Pacific Rise and Galapagos rift Sm-poor (<4 µg/g Sm) and low Ce/Sm (<0.7) glasses (**Figure 9**). Close to Kane Megamullion, such glasses have 49.5–51.9 wt.% SiO_2, Mg# of 0.67–0.51 (7–10 wt% MgO), Cr_2O_3 of 0.04–0.05 wt% and TiO_2 of 1.0 to 1.9 wt% [see Gale et al. (2013), and the PetDB (Lehnert et al., 2000) databases]. Close to Hess Deep, such glasses have SiO_2 ranging from 48.1 to 50.8 wt%, high Mg# of 0.69–0.62 (MgO: 8.5-10 wt%), high Cr_2O_3 (ca. 0.06 wt%) and low TiO_2 concentrations (0.9-1.2 wt%). Overall, Hess Deep clinopyroxene $core1_{HD}$ and plagioclase chadacrysts apparently crystallized from more primitive melt, at higher temperature than Kane Megamullion primocrysts.

Evidence for Gabbro Partial Melting

Clinopyroxene Core1 to Core2 Transition

The degree of partial mantle melting (e.g., Hirose and Kushiro, 1993) and mantle composition (e.g., Shimizu, 1998; Salters and Dick, 2002; Lambart et al., 2009) affect the basalt chemistry. Residual depleted lherzolite or harzburgite are REE- (especially LREE-), Zr-, Ti-depleted (Jochum et al., 1989) in comparison to lherzolite and may produce similar melt as core2 parental melt (**Figure 9**). However, higher degrees of peridotite partial

melting, either resulting from higher liquid fraction (F) and/or from partial melting of residual depleted lherzolite/harzburgite, produces a melt with higher Cr_2O_3 (Hirose and Kushiro, 1993) and lower Sr content, which thus fails to explain the core1 to core2 evolution. Melt compatible Cr_2O_3, Al_2O_3, Mg#, Sr/Sr* regularly decrease during fractionation of a gabbroic mineral assemblage, while incompatible TiO_2, Zr, Y and REE increase (e.g., Grove et al., 1992; Leuthold et al., 2015). Simple equilibrium or fractional crystallization thus fails to explain the geochemical zoning observed, which is characterized by decreases in Cr, Al, Zr, Y, REE and increases in Mg# and Sr/Sr* (**Figures 3**, **4**), thus pointing to incoherent behavior of compatible and incompatible elements.

Clinopyroxene oikocrysts from both the Kane Megamullion and Hess Deep show complex microtextures (**Figure 2**) associated with compositional zoning. The core1 to core2 contact is not related to the clinopyroxene crystalline structure but is wavy, with embayments developed especially along plagioclase chadacryst edges. For these reasons, we exclude the possibility that it results from sector zoning. Cooling and crystallization also fail to explain the clinopyroxene core1 resorption texture. Indeed, diffusion into an interstitial reactive melt fails to explain the sharp zonation pattern defined by the "immobile" elements (Cr, Ti, Al, REE) between core1 and core2. However, diffusion took place during protracted cooling of magma chambers, as shown by partly reequilibrated elements with higher diffusivities (e.g., Fe, Mg, Sr). Taken together, (1) the clinopyroxene resorption texture between core1 and core2; (2) the associated increase of Sr/Sr*; and (3) the plagioclase dissolution textures and reverse-zoning (**Figures 2B**, **7A**) all point to resorption of both clinopyroxene and plagioclase primocrysts and hence to gabbro dissolution. Olivine grains are in chemical equilibrium with the low Mg# clinopyroxene rim, assuming a D_{Fe-Mg} of 0.3 for olivine (Ulmer, 1989) and 0.24 for clinopyroxene (Bédard, 2010). Fe-Mg diffusion in olivine is fast and its primary composition has been chemically equilibrated, erasing any zoning that may have existed. The overgrowth of anhedral clinopyroxene core1 primocryst by the core2 oikocryst is best explained by gabbro partial dissolution, preferentially along grain boundaries, and subsequent crystallization from a distinct magma (i.e., different composition and temperature). We discuss the origin and composition of this magma in the next section.

Melt Hybridization at the Origin of the Clinopyroxene Core2

Lower oceanic crust gabbroic cumulates typically have higher Mg# (average of 82.6 at Hess Deep, Gillis et al., 2014a) and lower TiO_2 (0.04-0.59 wt%) (Coogan, 2014; Gillis et al., 2014a) and REE (especially LREE) (**Figure 6C**; see also Kelemen et al., 1997b) than the most primitive MORB glass [Mg# up to 0.68, TiO_2: 0.9–2.9 wt% (Gale et al., 2013); PetDB, (Lehnert et al., 2000)]. Thus, upon gabbro fractional crystallization, the melt Mg# would decrease and the incompatible TiO_2 and REE content would increase, at a slightly increasing Ce/Sm ratio (**Figure 9**). On the other hand, partial melting of gabbro cumulate produces a Ti-, Cr- and REE-poor melt with high Mg#. During increased or subsequent gabbro melting, the liquid progressively becomes more depleted in strongly incompatible elements (e.g., La, Ce) over moderately incompatible elements (e.g., Sm), thus resulting in a lower Ce/Sm ratio (**Figures 6C**, **9**). In comparison to the core1 parental melt, the clinopyroxene core2 parental melt is Ti-, Cr-, REE-poor, with a low Ce/Sm ratio, and has a high Mg#, as predicted by gabbro partial melting.

We calculated the gabbro protolith Sr concentration to be 100 μg/g and Sr/Sr* to be 7, using MELTS (Ghiorso and Sack, 1995) gabbro modal abundances and measured trace element compositions in plagioclase and clinopyroxene cores. MOR primitive glasses have Sr/Sr* values close to 0.8–1.5 (Gale et al., 2013 and PetDB, Lehnert et al., 2000 databases). Upon hybridization of anatectic gabbro melt with MOR primitive magma, the hybrid melt Sr/Sr* increases. The plagioclase stability field also expands (Leuthold et al., 2015) and results in an initial rapid Sr depletion along the hybrid melt liquid line of descent. We can speculate on the Sr/Sr* peak observed at the Hess Deep $core1_{HD}$-$core2_{HD}$ transition. The three analyses with Sr/Sr* up to 0.68 (see **Figure 4D**) are not related to a crack and far from any plagioclase inclusion. These high Sr/Sr* values might record plagioclase assimilation. The Kane Megamullion clinopyroxene experienced Sr diffusion over a few tenths to hundreds of micrometers upon cooling (**Figure 3D**), possibly erasing or attenuating sharp high Sr*/Sr peaks.

Geochemical modeling and basalt-gabbro isothermal reaction experiments show that modal partial melting of gabbroic cumulate produces a Cr-, Ti-, Zr-, REE-poor anatectic melt with high Mg# and Sr/Sr* (Leuthold et al., 2015; Leuthold and Ulmer, 2016). With a lower Ce/Sm ratio, the Kane Megamullion clinopyroxene $core2_{KM}$ most likely crystallized from a hybrid melt of such a gabbro partial melt with low Cr-, Zr- and REE- and high Mg# and newly injected mantle-derived primitive melt. We use Ce/Sm and Sm trace elements on **Figure 9**, to model the clinopyroxene core2 parental magma for both the Mid Atlantic Ridge and the East Pacific Rise samples (see **Table A.4** for calculations). The REE models show that the parental melts to clinopyroxene core2 are best explained by 10% modal equilibrium melting of gabbro (minerals mode estimated from MELTS calculations). However, we prefer a model where the core2 crystallized from a hybrid melt generated by mixing of gabbro anatectic melt (10–30%) with variable proportions of (depleted) lherzolite partial melt (10–20%). Likewise, spinel inclusions occurring along plagioclase chadacrysts within core2 may saturate following mixing and hybridization of a newly injected olivine-saturated magma with a cogenetic, differentiated, more siliceous melt (Irvine, 1977), such as anatectic gabbro or troctolite (Bédard et al., 2000; O'Driscoll et al., 2009; Leuthold et al., 2015). The sharp REE decrease from core1 to core2, if the latter crystallized from a hybrid melt, indicates that most if not all of the REE-rich trapped interstitial melt was lost prior to recrystallization. This would be the case if the gabbro protolith was either an adcumulate [e.g., ultra-slow-spreading Southwest Indian Ocean ridge (Gao et al., 2007 and references therein), fast-spreading ridge at Hess Deep (Natland and Dick, 1996)] or if it was a crystal mush and the interstitial melt was expelled prior to partial melting (e.g., Allibon et al., 2011).

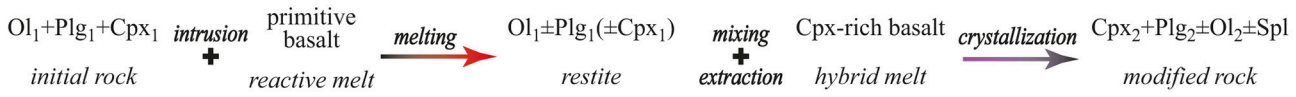

Figure 10 | Reaction showing gabbro (s.l.) partial melting and hybridization with hot mantle-derived melt. The lower oceanic crust gabbro (s.l.) and percolating MOR melts are physically and chemically modified. New and secondary phases will crystallize.

We propose that the clinopyroxene and plagioclase compositional data are best explained by partial melting of a gabbroic protolith (clinopyroxene core1 + plagioclase core and chadacrysts + olivine restite) that underwent intrusion/percolation by hot primitive mantle-derived melt. The products are a clinopyroxene-poor gabbro/troctolite residue and a hybrid melt saturated in clinopyroxene and plagioclase that subsequently crystallizes secondary clinopyroxene (core2 and rim) over rare relics and poikilitic gabbro calcic plagioclase (reversely zoned) rims (**Figure 10**). In addition, spinel may saturate in such hybrid basalt-silicic melts (Irvine, 1977; Bédard et al., 2000; O'Driscoll et al., 2009; Leuthold et al., 2015). This represents an alternative model for the petrogenesis of troctolite cumulate, classically interpreted as the product of low-pressure basalt fractional crystallization (see also Leuthold et al., 2014a; Coumans et al., 2016).

The partial melting-hybridization scenario for the origin of poikilitic gabbros is also consistent with the textural observations of clinopyroxene and plagioclase dissolution. During gabbro protolith partial melting, their stability increases in the basalt-gabbro hybrid melt (Leuthold et al., 2014a, 2015). Large oikocrysts may form in a clinopyroxene-poor groundmass by a crystal coarsening process (Mills et al., 2011), where abundant small nuclei are dissolved and recrystallized as fewer large oikocrysts over relic crystals. In the Hess Deep sample, the random orientation of plagioclase chadacrysts in the clinopyroxene core1$_{HD}$ and the preferred orientation of clinopyroxene rim$_{HD}$ plagioclase chadacrysts parallel to the main foliation (**Figures 1B**, **2D**; see also Gillis et al., 2014b) suggests crystallization of clinopyroxene core1$_{HD}$ predates cumulate compaction, while clinopyroxene rim$_{HD}$ postdates compaction. Leuthold et al. (2014a) interpreted similar textures in the Rum layered intrusion as the consequence of effective compaction-related grain alignment because of the porosity increase following melt percolation and partial melting.

The striking similarities of the crystal textures and mineral chemical traverses in the Kane Megamullion and Hess Deep poikilitic gabbros points convincingly to similar processes acting at slow- and fast-spreading ridges. Records of gabbro hybridization with mantle-derived melt have also been documented in ophiolites (Bédard et al., 2000). Furthermore, similar crystal textures and geochemical trends were documented in the Rum Layered Suite, where olivine-phyric and aphyric picritic sills (>1,200°C) intruded gabbroic cumulate (1,180–1,160°C), forming troctolitic restite and a clinopyroxene-saturated hybrid melt that percolated and refertilized the overlying gabbro, to produce poikilitic gabbro (Leuthold et al., 2014a, 2015). In addition, Coumans et al. (2016) demonstrated that melt inclusions in reversely-zoned plagioclase were trapped following melting and assimilation of plagioclase-rich cumulate by hot primitive mantle-derived melt (Juan de Fuca near-ridge seamount). Hence, partial melting of cumulates by invading melts may be a widespread (global) process. The implications for cumulates and melts in the lower oceanic crust are discussed in further detail below.

The Clinopyroxene Oikocryst Rims

The geochemical evolution of poikilitic gabbro clinopyroxene rims has been discussed in several studies and will only be briefly discussed here. The clinopyroxene oikocrysts show strong enrichments in incompatible elements (TiO_2, Zr and REE) and depletions in Cr_2O_3, Mg#, Eu/Eu* and Sr/Sr* toward their outer rims (**Tables A.1**, **A.2**). Such geochemical evolution is consistent with a fractional crystallization process. However, Lissenberg and MacLeod (2016) showed that fractional crystallization models fail to explain the observed outer rim enrichment, as well as the fractionation between incompatible elements. Previously published studies [e.g., Kane Fracture Zone in the Mid-Atlantic Ridge (Coogan et al., 2000; Lissenberg and MacLeod, 2016), Atlantis Bank in Southwest Indian Ridge (Gao et al., 2007; Lissenberg and MacLeod, 2016), Hess Deep in the Pacific Ocean (Lissenberg et al., 2013; Lissenberg and MacLeod, 2016)] explained the composition of the clinopyroxene outer rims by crystallization from pervasively infiltrated reactive differentiated melt. In that scenario, incompatible elements had been fractionated from one another by zone refining (e.g., McBirney, 1987) (chromatographic separation; a process by which a passing melt front depletes a solid framework in its incompatible elements through partial melting). Alternatively, Coogan and O'Hara (2015) modelled similar geochemical trends by *in situ* post-crystallization diffusive fractionation. Such late-stage processes are likely superimposed on the earlier and higher-temperature partial melting reactions described in this study.

The Troctolite–Medium-Grained Poikilitic Gabbro–Gabbro Suite

In the Kane Megamullion sample, the troctolite progressively grades to a medium-grained poikilitic gabbro and then to a gabbro (**Figure 1A**). In all three layers, the presence of similar normally zoned An-rich plagioclase (**Figure 7**) points to crystallization from a high temperature melt. Also interstitial clinopyroxene and clinopyroxene rims within the three lithologies have a similar chemistry (**Figure 5**). Finer-grained olivine and plagioclase in the troctolite at the contact with the coarse-grained poikilitic gabbro might suggest higher nucleation rates next to a colder rock. The troctolite appears to have differentiated *in situ* to a troctolite, a gabbro with interstitial clinopyroxene, and then to a gabbro. This suite may

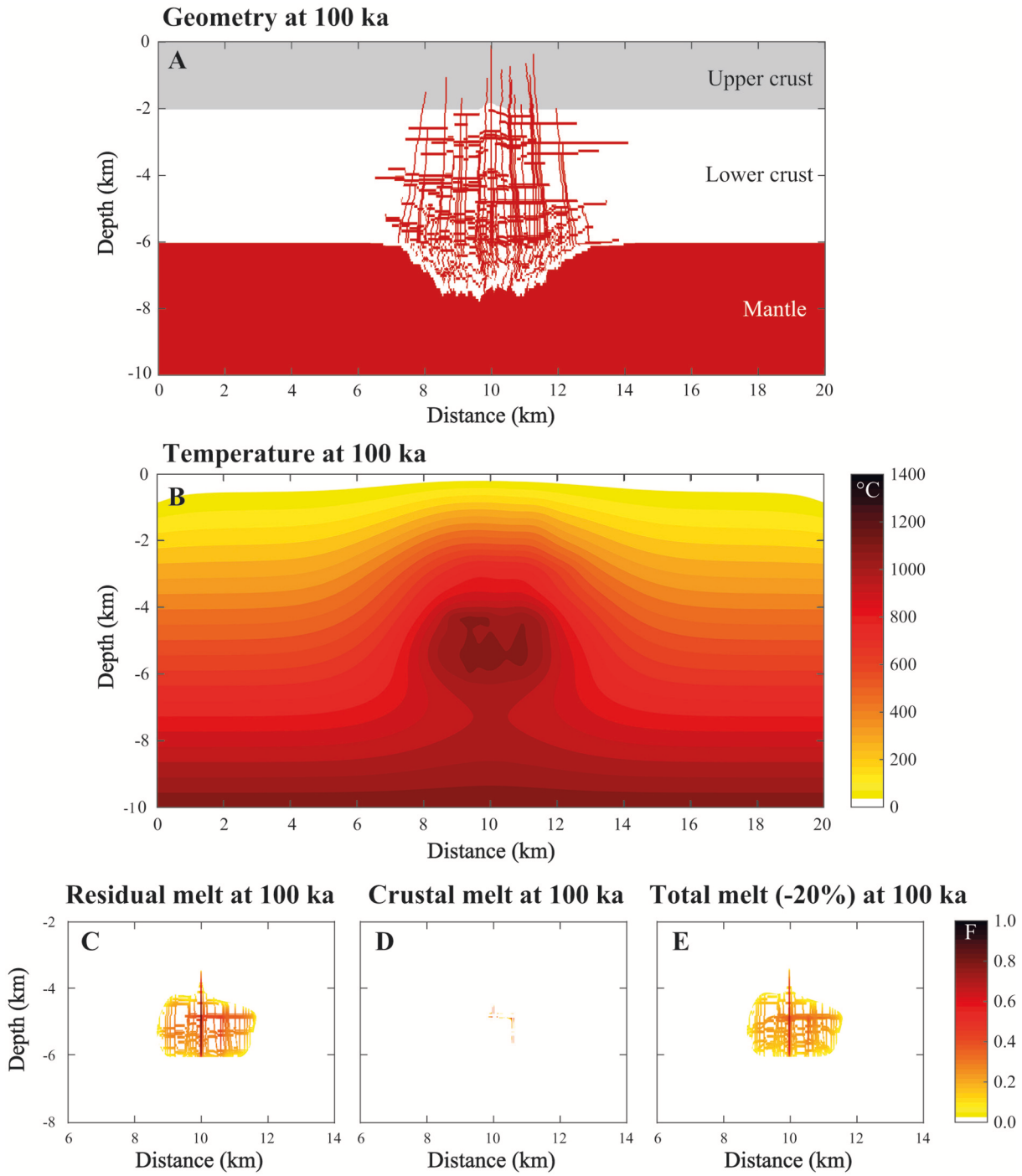

Figure 11 | Thermo-mechanical modeling of a slow-spreading ridge (spreading of 2 cm/year) (results for a similar model applied to fast-spreading ridges are shown in **Figure A.4**). **(A)** Dykes and sills intruded within the last 100′000 years (100 ka). **(B)** Thermal profile after 100 ka. It is very similar to the initial gradient, based on the Sinton and Detrick (1992) model. **(C)** Residual melt after cooling and crystallization of mantle-derived melt injected throughout the crust. **(D)** Crustal melt at 100 ka, localized next to dykes and sills. The occurrence of crustal melt is discontinuous in time. **(E)** Considering extraction of interstitial melt from the lower to the upper crust (estimated here to be ca. 20%), the total melt fraction is generally less than ca. 20%.

have crystallized from hot mantle-derived melt, percolating and melting the coarse-grained poikilitic gabbro. The gabbro clinopyroxene core composition is identical to the poikilitic gabbro clinopyroxene core2$_{KM}$, and distinct from the troctolite interstitial clinopyroxene (**Figure 5**). We suggest these grains were transferred from the poikilitic gabbro into the percolating

magma. Plagioclase rims in the coarse-grained poikilitic gabbro and troctolite have a similar chemical range (An_{81}-An_{68}) (**Figure 7**, **Table A.1**). They crystallized either from a mixture of anatectic gabbro and mantle-derived melts in variable proportions, or from a cooling and fractionating magma, similar to the troctolite.

Thermal Considerations

MELTS Models

Sufficient heat is needed for intrusive magma to partially melt a gabbroic cumulate, which requires specific conditions: (1) the gabbro cumulate must still be hot, (2) the temperature of the intruding melt must be higher than the solidus of the host gabbro cumulate, (3) the latent heat of fusion must not be much smaller than the latent heat of crystallization and (4) the mass ratio of assimilant to the invading hot melt must be low. We argue that each of these four conditions can be met: (1) Our MELTS (Ghiorso and Sack, 1995) calculations show gabbro (sensus stricto) fractionates from ca. 1,205 to ca. 1,155°C and we assume that the cumulate did not have sufficient time to cool to distinctly lower temperature (see **Figure 11**, **Figure A.4**; Sinton and Detrick, 1992); (2) Based on our textural observations and geochemical model above, we argue that the reactive hot basalt was not saturated in clinopyroxene or plagioclase. The solidus temperature of the mantle below mid-ocean ridges is estimated to ca. 1,250–1,280°C (e.g., Hirose and Kushiro, 1993; Hirschmann et al., 1998), which is higher than plagioclase and clinopyroxene saturation temperatures at crustal pressures (i.e., ca. 1,215°C); (3) As gabbro cumulate crystallized along the same liquid line of descent as the intruding hot primitive basalt, the latent heat of fusion and crystallization are likely to be similar (e.g., Sleep and Warren, 2014). The basalt latent heat of crystallization (ca. 12 kJ/g) released during dunite and troctolite crystallization is relatively low, as those cumulates represent only ca. 15 vol.% of total cumulate. (4) The exact volume of intruding melt is difficult to estimate, as magma injection is irregular and may occur over a protracted period of time. Indeed, White et al. (2012) showed magma injection into dykes occurs in pulses over weeks. Also, in their study of a dolerite sill, Holness and Humphreys (2003) pointed out conduits where magma may flux over months. As a result, wide contact aureoles and partial melting of the conduit wall can occur (e.g., Huppert and Sparks, 1989; Bruce and Huppert, 1990). Thirdly, magma may be repeatedly injected and drained back into the source region [e.g., Rum layered intrusion (O'Driscoll et al., 2007); Kilauea Iki lava lake (USGS)]. The potential for the host gabbro to melt thus mostly depends on its initial temperature and the temperature and volume of the intruding melt.

We have run MELTS (Ghiorso and Sack, 1995) isenthalpic assimilation models (energy constrained) to test the extent of gabbro cumulate assimilation. We present one realistic case here: 25 g of a gabbro assemblage fractionated at 1,175°C from mantle-derived melt at 150 MPa (see composition in **Table A.3**) and subsequently cooled down to 1,000°C, would be entirely assimilated by 100 g of mantle-derived melt intruded at 1,220°C. Upon complete assimilation, the liquid temperature would drop to 1,205°C (85 g left) and 40 g of solid phase would have fractionated. The saturation temperature of clinopyroxene is increased to 1,210°C, remains unchanged for plagioclase at 1,220°C and is decreased to 1,220°C for olivine. Isenthalpic models best represent continuous melting, crystallization and mixing processes, while isothermal models best represent natural situations where the assimilant melting and the invading melt crystallization precede mixing.

Thermal Modeling of the Crust

MELTS (Ghiorso and Sack, 1995) isenthalpic assimilation models do not consider intrusion geometry (e.g., distance to the intrusion) or the time evolution of heat diffusion process. For this reason, we ran simulations at the crustal scale using the Karakas and Dufek (2015) thermo-mechanical model, where the evolution of crustal and mantle-derived melts is investigated during dyke and sill intrusion in the crust. We modified the two-dimensional thermal model for the conditions of slow- and fast-spreading ridges and assumed an initial geometry constrained by Sinton and Detrick (1992). We simulated a computational domain of 10 km deep and 20 km wide (**Figure 11**, **Figure A.4A**) and assumed a crustal thickness of 6 km, with a 2 km upper crust and 4 km lower crust. We used two different initial temperature profiles (geotherms) that were based on the Sinton and Detrick models and the predicted isotherms of Dunn et al. (2000), for slow- and fast-spreading ridges respectively. We then simulated injection of 40 m thick dykes at different crustal levels, over a tectonic width of 4 km (**Figure 11A**, **Figure A.4A**), spreading the crust laterally. Dykes were intruded in a stochastic manner, corresponding to an average extension rate of 2 cm/year and 6 cm/year for slow- and fast-spreading ridges respectively. 80 m thick sills intruded in the lower crust, at dyke tips, thickening the crust. This effect is partly balanced by mantle upwelling at the base of the crust. The details of the thermal calculations and the methodology are explained in Karakas and Dufek (2015) and Karakas et al. (2017). To investigate the evolution of mantle-derived and crustal magmas during crystallization and melting, we used mantle-derived melt and crustal cumulate parameterized MELTS thermodynamic conditions. The mantle-derived melt liquid line of descent is identical to the one discussed above (see starting composition in **Table A.3**). The solidus temperature was set at 1,000°C, with a fixed crystallization rate of 0.3%/°C from 1,050°C. As a cumulate, the gabbroic crust solidus temperature was set at 1,150°C (i.e., above the pigeonite/orthopyroxene saturation temperature), assuming that interstitial melt was extracted at that temperature. Heat conduction drives crystallization of the dykes and sills and may generate partial melting of the host crust. The "residual melt" refers to the melt left behind after partial crystallization of mantle-derived melt (**Figure 11C**, **Figure A.4C**), while the "crustal melt" refers to the melt produced by partial melting of the crust (**Figure 11D**, **Figure A.4D**). On **Figure 11E** (**Figure A.4E**), the total melt (i.e., sum of residual melt and crustal melt) is reduced by 20% to account for interstitial melt extraction from the lower to the upper crust.

As spreading ridges are long-lived systems, the conductive geothermal gradient did not change significantly at the end of the simulations (i.e., after 100 ka) (**Figure 11B**, **Figure A.4B**).

The results of the thermal model show that partial melting of the crust occurs in the lower levels of the lower oceanic crust, adjacent to recently intruded dykes and sills. At slow-spreading ridges, crustal melting is low (< ca. 5% of the total melt volume) (**Figure 11D**) and not continuous over time. At fast-spreading ridges, residual melt is abundant, forming a vertically extensive zone of crystal mush. Crustal melt represents ca. 20 vol.% of the total melt volume (**Figure A.4D**). According to our calculations, the degree of partial melting in contact with dykes and sills can reach ca. 50% locally (i.e., corresponding to a temperature increase to ca. 1,170°C). Our thermal models confirm the above microtextural and geochemical observations of gabbro partial melting. In **Figure 11E**, **Figure A.4E**, the total melt is estimated to be generally less than 20% in slow-spreading ridges and less than 40% in fast-spreading ridges, after partial extraction of melt from the lower crust to the upper crustal level and seafloor.

Effect of Gabbro Partial Melting on Mantle-Derived Melt

The mineralogy and chemical composition of the cogenetic MOR melt and assimilated young oceanic gabbro are not significantly different. It is thus difficult to detect the assimilation of mafic cumulates in MORB. We discuss here the effects of gabbro assimilation on the mineral assemblage, the major element chemistry and the REE chemistry of the hybrid melt.

Mineral Stability and Major Element Chemistry

Koepke et al. (2004) showed that partial melting of hydrated gabbro at 900–950°C, with clinopyroxene reaction to orthopyroxene and pargasitic amphibole, produces felsic melt at the origin of the plagiogranite. Through isothermal assimilation of dry primitive gabbro, the hybrid melt liquid line of descent is shifted toward higher SiO_2, Mg#, CaO and Al_2O_3 values (**Figure 8**; Leuthold et al., 2015). The stability of clinopyroxene and plagioclase is increased. Due to the increase in SiO_2, the olivine stability is decreased, replaced by orthopyroxene, which might occur as a cumulus phase even in primitive gabbro, as observed in the Hess Deep drilled cores (Gillis et al., 2014a,b). It also results in a Mg# increase in clinopyroxene (Bédard, 2010; Leuthold et al., 2015). High temperature cumulate also has low TiO_2, FeO_T, Na_2O, K_2O, which are consequently low in the hybrid melt.

We also used MELTS (Ghiorso and Sack, 1995) to quantify the effect of gabbro assimilation on the major element chemistry of mantle-derived melt (e.g., Leuthold et al., 2014a; Coumans et al., 2016). Models are shown on the **Figure 8**. The effect of 50% gabbro cumulate partial melting and subsequent mixing with mantle-derived melt differentiated to 1,200°C (see compositions of anatectic melt and differentiated mantle-derived melt in **Table A.3**) is similar to a pressure decrease of ca. 100 MPa, a water increase of ca. 0.3 wt.%, a redox state change from NNO-2 to NNO-0.5 (i.e., more oxidized) or non-ideal fractional crystallization (i.e., with limited equilibrium crystallization).

REE Chemistry

MORB and lower crust clinopyroxene may show a wide range of REE, from REE-poor N-MORB (i.e., $Ce/Sm)_N$ <1.00) to REE-rich E-MORB (i.e., $Ce/Sm)_N$ >1.00) as a result of compositional heterogeneity in the mantle source and variation in partial melting processes (e.g., Kelemen et al., 1997a). Indeed, low-grade partial melting of a fertile lherzolite (not previously molten) or a refertilized peridotite would produce a REE-rich basalt with Ce/Sm_N >1 (**Figure 9**). Upon further melting, the residue and melt REE concentration and Ce/Sm ratio progressively decrease. Partial melting of such a residual peridotite (i.e., depleted lherzolite, harzburgite) would produce melt with a low Ce/Sm_N ratio (typically <1) (**Figure 9**). In the Hirose and Kushiro (1993) partial melting experiments of the relatively fertile KLB-1 spinel-lherzolite at 1.5 GPa, the solidus temperature is ca. 1,280°C and the clinopyroxene is totally molten between 1,350 and 1,400°C (i.e., leaving a harzburgitic residue), corresponding to a liquid fraction of 19–29%. pMELTS (Ghiorso et al., 2002) calculations using KLB-1 lherzolite composition at 1.5 GPa show that clinopyroxene is totally molten after 23% partial melting, at 1,455°C.

The gabbro cumulates are REE-poor, with low Ce/Sm ratios (Kelemen et al., 1997b), in comparison to mantle-derived melt compositions (**Figure 6C**). Upon crystal fractionation, differentiated MOR melts become REE-enriched. Conversely, gabbro cumulate partial melting produces a REE-poor melt with low Ce/Sm (**Figure 9**). In addition, upon increased gabbro melting, the clinopyroxene-hybrid melt REE partition coefficient will decrease (Leuthold and Ulmer, 2016), increasing the effect of REE depletion. When considering the REE concentrations of MOR melts, it is difficult to distinguish between assimilation of low REE gabbro and higher degrees of partial melting of lherzolite or depleted-lherzolite, particularly since primary melts are unlikely to exist.

CONCLUSIONS

We conclude that the oceanic lower crust poikilitic gabbros studied here record: (1) intrusion of hot mantle-derived primitive melt into the young, still-hot gabbroic lower oceanic crust, (2) cooling and crystallization of the intrusive magma and partial melting of the host gabbro cumulate to an equilibrium temperature, (3) mixing of the two melts, (4) possible extraction and percolation of the hybrid melt, (5) crystallization of secondary phases (e.g., clinopyroxene core2 and rim and plagioclase rim) and saturation of new phases (e.g., spinel) (i.e., refertilization) (see **Graphical Abstract**, **Figure 10**). Partial melting has affected primocrysts and modified the composition and textures (i.e., mineral modes, intra-crystal textures) of the lower oceanic gabbro cumulate, producing pyroxene-poor gabbro/troctolite residue and a hybrid melt [Cr-, Al-, REE-(especially LREE-) poor and with high Mg#] saturated in clinopyroxene and plagioclase. Importantly, the observations made here suggest that a similar MASH process operates in slow- and fast-spreading ridges, as well as in layered intrusions (see Leuthold et al., 2014a) and arcs (e.g., Hildreth and Moorbath, 1988; Cooper et al., 2016). Thermal models confirm (locally high degree) partial melting of hot gabbro cumulate by recently intruded dykes and sills. However, the overall volume of crustal melt is low.

MORB magmas commonly have high Mg#, low REE concentrations and low Ce/Sm ratios. The Atlantic, East Pacific

Rise and Galapagos major elements trends of natural glass follow liquid lines of descent from unmodified mantle-derived melts, extracted from variable depths. However, lower oceanic gabbro clinopyroxene oikocrysts and plagioclase microtextures and zoning point to hybridization of primitive magmas with oceanic crustal gabbro. The process of gabbro assimilation described here contributes to the large chemical variability of MORB at conditions close to the liquidus, in addition to mantle partial melting processes and crystallization at mantle and crustal depths. However, the lack of strong mineralogical and/or geochemical contrasts between co-genetic invading basaltic melt and gabbro cumulate makes it difficult to distinguish in erupted MOR lavas alone. Great care is therefore required to show modification during percolation through the lower oceanic crust filter, when only considering MORB major and trace elements. Discerning and quantifying possible reactions of primitive mantle-derived melt with lower oceanic crust is critical in the interpretation of oceanic basalt compositions, in order to avoid inadequate petrogenetic models derived from the incorrect assumption of equilibrium premises (e.g., degree of mantle partial melting deduced from the MORB geochemistry proxy). Further studies are necessary to evaluate how pervasive the MASH process is during the generation and differentiation of the oceanic crust.

AUTHOR CONTRIBUTIONS

JL has initiated the research project, analyzed samples and supervised M.Sc. student DK at every step. He has run the MELTS calculations, done the geochemical modeling and helped with the thermal modeling. He has written the manuscript and prepared the figures. CL has conducted detailed microscopic and geochemical study on the studied Kane Megamullion sample. He has helped writing the manuscript. BO has helped writing the manuscript. OK has written and run the thermal models. TF has provided the Hess Deep sample. He had acquired preliminary SEM images. DK has prepared the samples. She has helped acquiring preliminary SEM images and EMPA analyses and reducing LA-ICP-MS data. PU helped to initiate the project. We had fruitful discussions and he helped writing the manuscript. All authors have approved this submitted version.

FUNDING

This study was supported by the Swiss National Science Foundation (SNSF) Ambizione grant (PZ00P2_161206/1) to JL. CL was supported by NERC Grant NE/I001670/1. BO acknowledges support from a Royal Society Research Grant (RG100528) and from Natural Environment Research Council (NERC) New Investigator grant NE/J00457X/1 and Standard Grant NE/L004011/1. OK acknowledges the support from SNSF project 200020_165501. TF acknowledges funding from ANZIC and the ARC.

ACKNOWLEDGMENTS

We thank Lukas Martin for assistance with EMPA and Marcel Guillong for assistance with LA-ICP-MS. Comments by Matthieu Galvez, Tomoaki Morishita, Laurence Coogan and others helped to improve a former version of this paper. This research used samples collected during the R/V Knorr cruise 180-2 in the Fall of 2004 and the International Ocean Discovery Program (IODP) expedition 345 in Winter of 2012. We acknowledge the crews and the science party. Mark Ghiorso's class on MELTS was really helpful. We appreciate insightful comments of Josef Dufek and Olivier Bachmann on thermal modeling over the years.

SUPPLEMENTARY MATERIAL

The Supplementary Material for this article can be found online at: https://www.frontiersin.org/articles/10.3389/feart.2018.00015/full#supplementary-material

Figure A.1 | JAS117-63 sample. From left to right, layers of gabbro grading to a medium-grained poikilitic gabbro with interstitial clinopyroxene, to a fine-grained troctolite, in contact with a coarse-grained poikilitic gabbro.

Figure A.2 | U1415I_4R_2_9-13 sample (see Gillis et al., 2014b). Clinopyroxene oikocrysts in a foliated troctolitic groundmass.

Figure A.3 | (A) Kane Megamullion and **(B)** Hess Deep complex clinopyroxene microtextures revealed by EMPA X-ray TiO_2 maps. See also **Figure 2**.

Figure A.4 | Thermo-mechanical modeling of a fast-spreading ridge (spreading of 6 cm/year) (see also **Figure 11** for thermal modeling of a slow-spreading ridge). **(A)** Dykes and sills intruded within the last 100 ka. **(B)** Thermal profile after 100 ka. It is very similar to the initial gradient, based on Sinton and Detrick (1992) model. **(C)** Residual melt after cooling and crystallization of mantle-derived melt injected throughout the crust. **(D)** Crustal melt at 100 ka, localized next to dykes and sills. The occurrence of crustal melt is discontinuous in time. **(E)** Considering extraction of interstitial melt from the lower to the upper crust (estimated here to be ca. 20%), the total melt fraction is generally less than ca. 40%.

Table A.1 | Kane Megamullion JAS117-63 poikilitic gabbro and troctolite EMPA major and LA-ICP-MS trace element mineral data.

Table A.2 | Hess Deep 345_U1415I-4R_2_9-13 poikilitic gabbro EMPA major and LA-ICP-MS trace element mineral data.

Table A.3 | Melt, gabbro and fertile spinel lherzolite compositions used in the geochemical models of **Figure 9**.

Table A.4 | Fertile spinel lherzolite, depleted lherzolite, harzburgite and gabbro partial melting REE geochemical modeling.

Presentation 1 | Interactive microscopic view of the Mid-Atlantic ridge Kane Megamullion JAS117-63 gabbroic sample. In the slide show mode, use red buttons to change from plan polarized light (PPL) to cross polarized light (XPL), zoom in and out and rotate the sample.

REFERENCES

Abily, B., and Ceuleneer, G. (2013). The dunitic mantle-crust transition zone in the Oman ophiolite: residue of melt-rock interaction, cumulates from high-MgO melts, or both? *Geology* 41, 67–70. doi: 10.1130/G33351.1

Allibon, J., Bussy, F., Lewin, E., and Darbelley, B. (2011). The tectonically controlled emplacement of a vertically sheeted gabbro-pyroxenite intrusion: feeder-zone of an ocean-island volcano (Fuerteventura, Canary Islands). *Tectonophysics* 500, 78–97. doi: 10.1016/j.tecto.2010.01.011

Bédard, J. H. (2010). Parameterization of the Fe=Mg exchange coefficient (Kd) between clinopyroxene and silicate melts. *Chem. Geol.* 274, 169–176. doi: 10.1016/j.chemgeo.2010.04.003

Bédard, J. H. (2014). Parametrizations of calcic clinopyroxene – melt trace element partition coefficients. *Geochem. Geophys. Geosyst.* 15, 303–336. doi: 10.1002/2013GC005112

Bédard, J., Hébert, R., Berclaz, A., and Varfalvy, V. (2000). "Syntexis and the genesis of oceanic crust," in *Ophiolites and Oceanic Crust: New Insights from Field Studies and the Ocean Drilling Program, Geological Society of America Special Paper,* eds D. Yildrim, E. Moores, D. Elthon, and A. Nicolas (Boulder, CO), 105–119.

Boynton, W. V. (1984). Cosmochemistry of the rare earth elements: meteorite studies, in *Rare Earth Element Geochemistry,* ed P. E. Hendersen (Amsterdam: Elsevier), 63–114.

Bruce, P. M., and Huppert, H. E. (1990). "Solidification and melting along dykes by the laminar flow of basaltic magma," in *Magma Transport and Storage,* ed M. P. Ryan (Chichester: John Wiley), 87–101.

Clog, M., Aubaud, C., Cartigny, P., and Dosso, L. (2013). The hydrogen isotopic composition and water content of southern Pacific MORB: a reassessment of the D/H ratio of the depleted mantle reservoir. *Earth. Planet. Sci. Lett*. 381, 156–165. doi: 10.1016/j.epsl.2013.08.043

Collier, M. L., and Kelemen, P. B. (2010). The case for reactive crystallization at mid-ocean ridges. *J. Petrol*. 51, 1913–1940. doi: 10.1093/petrology/egq043

Coogan, L. A. (2014). "The lower oceanic crust," in *The Crust. Treatise on Geochemistry*, ed R. L. Rudnick (Elsevier), 497–541.

Coogan, L. A., and O'Hara, M. J. (2015). MORB differentiation: *in situ* crystallization in replenished-tapped magma chambers. *Geochem. Cosmochem. Ac*. 158, 147–161. doi: 10.1016/j.gca.2015.03.010

Coogan, L. A., Saunders, A. D., Kempton, P. D., and Norry, M. J. (2000). Evidence from oceanic gabbros for porous melt migration within a crystal mush beneath the Mid-Atlantic Ridge. *Geochem. Geophys. Geosyst.* doi: 10.1029/2000GC000072

Coogan, L. A., Thompson, G., and MacLeod, C. J. (2002). A textural and geochemical investigation of high level gabbros from the Oman ophiolite: implications for the role of the axial magma chamber at fast-spreading ridges. *Lithos* 63, 67–82. doi: 10.1016/S0024-4937(02)00114-7

Cooper, G. F., Davidson, J. P., and Blundy, J. D. (2016). Plutonic xenoliths from Martinique, Lesser Antilles: evidence for open system processes and reactive melt flow in island arc crust. *Contrib. Mineral. Petrol*. 171:87. doi: 10.1007/s00410-016-1299-8

Coumans, J. P., Stix, J., Clague, D. A., Minarik, W. G., and Layne, G. D. (2016). Melt-rock interaction near the Moho: evidence from crystal cargo in lavas from near-ridge seamounts. *Geochem. Cosmochem. Ac*. 191, 139–164. doi: 10.1016/j.gca.2016.07.017

De Paolo, D. J. (1981). Trace element and isotopic effects of combined wallrock assimilation and fractional crystallization. *Earth Planet. Sci. Lett*. 53, 189–202. doi: 10.1016/0012-821X(81)90153-9

Dick, H. J. B., Tivey, M. A., and Tucholke, B. E. (2008). Plutonic foundation of a slow-spreading ridge segment: oceanic core complex at Kane Megamullion, 23°30'N, 45°20'W. *Geochem. Geophys. Geosyst*. 9, 44. doi: 10.1029/2007GC001645

Donaldson, C. H. (1985). The rates of dissolution of olivine, plagioclase and quartz in a basalt melt. *Mineral. Mag*. 49, 683–693. doi: 10.1180/minmag.1985.049.354.07

Dungan, M. A., and Rhodes, J. M. (1978). Residual glasses and melt inclusions in basalts from DSDP legs 45 and 46: evidence for magma mixing. *Contrib. Mineral. Petrol*. 67, 417–431. doi: 10.1007/BF00383301

Dunn, R. A., Toomley, D. R., and Solomon, S. C. (2000). Three-dimensional seismic structure and physical properties of the crust and shallow mantle beneath the East Pacific Rise at 9°30'N. *J. Geophys. Res*. 105, 23537–23555. doi: 10.1029/2000JB900210

Eason, D. E., and Sinton, J. M. (2009). Lava shields and fissure eruptions of the Western volcanic zone, Iceland: evidence for magma chambers and crustal interaction. *J. Volcanol. Geotherm. Res*. 186, 331–348. doi: 10.1016/j.jvolgeores.2009.06.009

Elthon, D. (1979). High magnesian liquids as the parental magma for ocean floor basalts. *Nature* 278, 514–518. doi: 10.1038/278514a0

Feig, S., Koepke, J., and Snow, J. (2006). Effect of water on tholeiitic basalt phase equilibria: an experimental study under oxidizing conditions. *Contrib. Mineral. Petrol*. 152, 611–638. doi: 10.1007/s00410-006-0123-2

Francheteau, J., Armiho, R., Cheminee, J. L., Hekinian, R., Lonsdale, P., and Blumm, N. (1990). 1Ma East Pacific rise oceanic crust and uppermost mantle exposed by rifting in Hess Deep (equatorial Pacific Ocean). *Earth Planet. Sci. Lett*. 101, 281–295. doi: 10.1016/0012-821X(90)90160-Y

Gale, A., Dalton, C. A., Langmuir, C. H., Su, Y., and Schilling, J.-G. (2013). The mean composition of ocean ridge basalts. *Geochem. Geophys. Geosyst*. 14, 489–518. doi: 10.1029/2012GC004334

Gao, Y., Hoefs, J., Hellebrand, E., von der Handt, A., and Snow, J. E. (2007). Trace element zoning in pyroxenes from ODP Hole 735B gabbros: diffusive exchange or synkinematic crystal fractionation? *Contrib. Mineral. Petrol*. 153, 429–442. doi: 10.1007/s00410-006-0158-4

Ghiorso, M. S., Hirschmann, M. M., Reiners, P. W., and Kress, V. C. III. (2002). The pMELTS: a revision of MELTS aimed at improving calculation of phase relations and major element partitioning involved in partial melting of the mantle at pressures up to 3 GPa. *Geochem. Geophys. Geosyst*. 3, 1–35. doi: 10.1029/2001GC000217

Ghiorso, M. S., and Sack, R. O. (1995). "Chemical mass transfer in magmatic processes IV. A revised and internally consistent thermodynamic model for the interpolation and extrapolation of liquid-solid equilibria in magmatic systems at elevated temperatures and pressures. *Contrib. Mineral. Petrol*. 119, 197–212. doi: 10.1007/BF00307281

Gillis, K. M., Snow, J. E., Klaus, A., Abe, N., Adrião, A. B., Akizawa, N., et al. (2014a). Primitive layered gabbros from fast-spreading lower oceanic crust. *Nature* 505, 204–208. doi: 10.1038/nature12778

Gillis, K. M., Snow, J. E., Klaus, A., Guerin, G., Abe, N., Akizawa, N., et al. (2014b). "Hole U1415J," in *Proceedings of IODP*, eds K. M. Gillis, J. E. Snow, A. Klaus, and the Expedition 345 Scientists (College Station, TX: Integrated Ocean Drilling Program).

Grove, T. L., and Bryan, W. B. (1983). Fractionation of pyroxene-phyric MORB at low pressure: an experimental study. *Contrib. Mineral. Petrol*. 84, 293–309. doi: 10.1007/BF01160283

Grove, T. L., Kinzler, R. J., and Bryan, W. B. (1992). Fractionation of Mid-Ocean Ridge Basalt (MORB). *Geophys. Monogr. Ser*. 71, 281–310. doi: 10.1029/GM071p0281

Guillong, M., Meier, D. M., Allan, M. M., Heinrich, C. A., and Yardley, B. W. D. (2008). "SILLS: a Matlab-based program for the reduction of laser ablation ICP-MS data of homogeneous materials and inclusions," in *Laser-Ablation-ICPMS in the Earth Sciences: Current Practices and Outstanding Issues*, ed P. Sylvester (Vancouver, BC: Mineralogical Association of Canada), 328–333.

Hildreth, W., and Moorbath, S. (1988). Crustal contributions to arc magmatism in the Andes of Central Chile. *Contrib. Mineral. Petrol*. 98, 455–489. doi: 10.1007/BF00372365

Hirose, K., and Kushiro, I. (1993). Partial melting of dry peridotites at high pressures: determination of compositions of melts segregated from peridotite using aggregates of diamond. *Earth Plant. Sci. Lett*. 114, 477–489. doi: 10.1016/0012-821X(93)90077-M

Hirschmann, M. M., Ghiorso, M. S., Wasylenki, L. E., Asimow, P. D., and Stolper, E. M. (1998). Calculation of peridotite partial melting from thermodynamic models of minerals and Melts. Review of methods and comparison with experiments. *J. Petrol*. 39, 1091–1115. doi: 10.1093/petroj/39.6.1091

Holloway, M. I., and Bussy, F. (2008). Trace element distribution among rock-forming minerals from metamorphosed to partially molten basic igneous rocks in a contact aureole (Fuerteventura, Cararies). *Lithos* 102, 616–639. doi: 10.1016/j.lithos.2007.07.026

Holness, M. B., and Humphreys, M. C. S. (2003). The Traigh Bhàn na Sgùrra sill, Isle of Mull: flow localization in a major magma conduit. *J. Petrol*. 44, 1961–1976. doi: 10.1093/petrology/egg066

Huppert, H. E., and Sparks, R. S. J. (1989). Chilled margins in igneous rocks. *Earth Planet. Sci. Lett*. 92, 397–405. doi: 10.1016/0012-821X(89)90063-0

Irvine, T. N. (1977). Origin of chromite layers in the Muskox intrusion and other stratiform intrusions: a new perspective. *Geology* 5, 273–277. doi: 10.1130/0091-7613(1977)5<273:OOCLIT>2.0.CO;2

Jochum, K. P., McDonough, W. F., Palme, H., and Spettel, B. (1989). Compositional constraints on the continental lithospheric mantle from

trace elements in spinel peridotite xenoliths. *Nature* 340, 548–550. doi: 10.1038/340548a0

Karakas, O., and Dufek, J. (2015). Melt evolution and residence in extending crust: thermal modeling of the crust and crustal magmas. *Earth Planet. Sci. Lett*. 425, 131–144. doi: 10.1016/j.epsl.2015.06.001

Karakas, O., Dufek, J., Mangan, M. T., Wright, H. M., and Bachmann, O. (2017). Thermal and petrologic constraints on lower crustal melt accumulation under the Salton Sea Geothermal Field. *Earth Planet. Sci. Lett.* 467, 10–17. doi: 10.1016/j.epsl.2017.02.027

Kelemen, P. B., Hirth, G., Shimizu, N., Spiegelman, M., and Dick, H. J. B. (1997a). A review of melt migration processes in the adiabatically upwelling mantle beneath oceanic spreading ridges. *Philos. Trans. R. Soc. Lond. A* 355, 283–318. doi: 10.1098/rsta.1997.0010

Kelemen, P. B., Koga, K., and Shimizu, N. (1997b). Geochemistry of gabbro sills in the crust-mantle transition zone of the Oman ophiolite: implications for the origin of the oceanic lower crust. *Earth Planet. Sci. Lett.* 146, 475–488. doi: 10.1016/S0012-821X(96)00235-X

Klein, E. M., and Langmuir, C. H. (1987). Global correlations of ocean ridge basalt chemistry with axial depth and crustal thickness. *J. Geophys. Res*. 92, 8089–8115. doi: 10.1029/JB092iB08p08089

Koepke, J., Feig, S. T., Snow, J., and Freise, M. (2004). Petrogenesis of oceanic plagiogranites by partial melting of gabbros: an experimental study. *Contrib. Mineral. Petrol*. 146, 414–432. doi: 10.1007/s00410-003-0511-9

Kvassnes, A., and Grove, T. (2008). How partial melts of mafic lower crust affect ascending magmas at oceanic ridges. *Contrib. Mineral. Petrol*. 156, 49–71. doi: 10.1007/s00410-007-0273-x

Lambart, S., Laporte, D., and Schiano, P. (2009). An experimental study of pyroxenite partial melts at 1 and 1.5 GPa: implications for the major-element composition of mid-ocean Ridge basalts. *Earth Planet. Sci. Lett*. 288, 335–347. doi: 10.1016/j.epsl.2009.09.038

Laubier, M., Gale, A., and Langmuir, C. H. (2012). Melting and crustal processes at the FAMOUS segment (Mid-Atlantic Ridge): new insights from olivine-hosted melt inclusions from multiple samples. *J. Petrol*. 53, 665–698. doi: 10.1093/petrology/egr075

Lehnert, K., Su, Y., Langmuir, C. H., Sarbas, B., and Nohl, U. (2000). A global geochemical database structure for rocks. *Geochem. Geophys. Geosyst*. 1, 1–14. doi: 10.1029/1999GC000026

Leuthold, J., Blundy, J. D., and Brooker, R. A. (2015). Experimental petrology constraints on the recycling of mafic cumulate: a focus on Cr-spinel from the Rum Eastern layered intrusion, Scotland. *Contrib. Mineral. Petrol*. 170:12. doi: 10.1007/s00410-015-1165-0

Leuthold, J., Blundy, J. D., Holness, M. B., and Sides, R. (2014a). Successive episodes of reactive liquid flow through a layered intrusion (Unit 9, Rum Eastern layered intrusion, Scotland). *Contrib. Mineral. Petrol*. 167, 1–27. doi: 10.1007/s00410-014-1021-7

Leuthold, J., Müntener, O., Baumgartner, L. P., and Putlitz, B. (2014b). Petrological constraints on the recycling of mafic crystal mushes and intrusion of braided sills in the Torres del Paine mafic complex (Patagonia). *J. Petrol.* 55, 917–949. doi: 10.1093/petrology/egu011

Leuthold, J., and Ulmer, P. (2016). "High temperature crystal-melt reaction in mafic igneous complexes," in *EMPG Meeting Abstract* (Zürich).

Lissenberg, C. J., and Dick, H. J. B. (2008). Melt–rock reaction in the lower oceanic crust and its implications for the genesis of mid-ocean ridge basalt. *Earth Planet. Sci. Lett*. 271, 311–325. doi: 10.1016/j.epsl.2008.04.023

Lissenberg, C. J., and MacLeod, C. J. (2016). A reactive porous flow control on the Mid-ocean ridge magmatic evolution. *J. Petrol.* 57, 2195–2220. doi: 10.1093/petrology/egw074

Lissenberg, C. J., MacLeod, C. J., Horward, K. A., and Godard, M. (2013). Pervasive reactive melt migration through fast-spreading lower oceanic crust (Hess Deep, equatorial Pacific Ocean). *Earth Planet. Sci. Lett*. 361, 436–447. doi: 10.1016/j.epsl.2012.11.012

McBirney, A. R. (1987). "Constitutional zone refining of layered intrusions," in *Origins of Igneous Layering*, Vol. 196, ed I. Parsons (Dordrecht: D. Reidel Publishing Company), 437–452.

Miller, D. J., Abratis, M., Christie, D., Drouin, M., Godard, M., Ildefonse, B., et al. (2009). "Data report: microprobe analyses of primary mineral phases from Site U1309, Atlantis Massif, IODP Expedition 304/305," in *Proceedings of IODP 304/305*, eds D. K. Blackman, B. Ildefonse, B. E. John, Y. Ohara, D. J. Miller, and C. J. MacLeod (Integrated Ocean Drilling Program Management International). doi: 10.2204/iodp.proc.304305.202.2009

Mills, R. D., Ratner, J. J., and Glazner, A. F. (2011). Experimental evidence for crystal coarsening and fabric development during temperature cycling. *Geology* 39, 1139–1142. doi: 10.1130/G32394.1

Natland, J. H., and Dick, H. J. B. (1996). "ODP. Melt migration through high-level gabbroic cumulates of the East Pacific Rise at Hess Deep: the origin of magma lenses and the deep crustal structure of fast-spreading ridges," in *Proceedings of the ODP Science Results*, eds C. Mevel, K. M. Gillis, and J. F. Allan (College Station, TX: Ocean Drilling Program), 21–58.

O'Driscoll, B., Emeleus, C. H., Donaldson, C. H., and Daly, J. S. (2009). The roles of melt infiltration and cumulate assimilation in the formation of anorthosite and a Cr-spinel seam in the Rum Eastern layered intrusion, NW Scotland. *Lithos* 111, 6–20. doi: 10.1016/j.lithos.2008.11.011

O'Driscoll, B., Hagraves, R. B., Emeleus, C. H., Troll, V. R., Donaldson, C. H., and Reavy, R. J. (2007). Magmatic lineations inferred from anisotropy of magnetic susceptibility fabrics in Units 8, 9, and 10 of the Rum Eastern layered series, NW Scotland. *Lithos* 98, 27–44. doi: 10.1016/j.lithos.2007.01.009

O'Neill, H. S., and Jenner, F. E. (2012). The global pattern of trace-element distributions in ocean floor basalts. *Nature* 491, 698–705. doi: 10.1038/nature11678

Quick, J. E. (1981). The origin and significance of large, tabular dunite bodies in the trinity peridotite, northern California. *Contrib. Mineral. Petrol*. 78, 413–422. doi: 10.1007/BF00375203

Ridley, W. I. M. R., Perfit, M. C., and Smith, D. J. (2006). Fornari magmatic processes in developing oceanic crust revealed in a cumulate xenolith collected at the East pacific rise, 9–50°N. *Geochem. Geophys. Geosyst*. 7:Q12OQ04. doi: 10.1029/2006GC001316

Righter, K., Drake, M. J., and Scott, E. (2006). "Compositional relationships between meteorites and terrestrial planets," in *Meteorites and the Early Solar System II,* eds D. S. Lauretta and H. Y. McSween, (Tucson, AZ: University of Arizona Press), 803–828.

Salters, V. J. M., and Dick, H. J. B. (2002). Mineralogy of the mid-ocean-ridge basalt source from neodymium isotopic composition of abyssal peridotites. *Nature* 418, 68–72. doi: 10.1038/nature00798

Sanfilippo, A., Tribuzio, R., Tiepolo, M., and Berno, D. (2015). Reactive flow as dominant evolution process in the lowermost oceanic crust: evidence from olivine of the Pineto ophiolite. *Contrib. Mineral. Petrol*. 170:38. doi: 10.1007/s00410-015-1194-8

Shimizu, N. (1998). The geochemistry of olivine-hosted melt inclusions in a Famous basalt ALV519-4-1. *Phys. Earth Planet In*. 107, 183–201. doi: 10.1016/S0031-9201(97)00133-7

Shorttle, O. (2015). Geochemical variability in MORB controlled by concurrent mixing and crystallization. *Earth Planet. Sci. Lett*. 424, 1–14. doi: 10.1016/j.epsl.2015.04.035

Sinton, J., and Detrick, R. (1992). Mid-ocean ridge magma chambers. *J. Geophys. Res*. 97, 197–216. doi: 10.1029/91JB02508

Sleep, N. H., and Warren, J. M. (2014). Effect of latent heat of freezing on crustal generation at low spreading rates. *Geochem. Geophys. Geosyst*. 15, 3161–3174. doi: 10.1002/2014GC005423

Sobolev, A. V., and Shimizu, N. (1993). Ultra-depleted primary melt included in an olivine from the Mid-Atlantic Ridge. *Nature* 363, 151–154. doi: 10.1038/363151a0

Solano, J. M. S., Jackson, M. D., Sparks, R. S. J., Blundy, J. D., and Annen, C. (2012). Melt segregation in deep crustal hot zones: a mechanism for chemical differentiation, crustal assimilation and the formation of evolved magmas. *J. Petrol*. 53, 1999–2026. doi: 10.1093/petrology/egs041

Thy, P., Lesher, C. E., Nielsen, T. F. D., and Brooks, C. K. (2006). Experimental constraints on the Skaergaard liquid line of descent. *Lithos* 92, 154–180. doi: 10.1016/j.lithos.2006.03.031

Tormey, D. R., Grove, T. L., and Bryan, W. B. (1987). Experimental petrology of normal MORB near the Kane Fracture Zone: 22°–25° N, mid-Atlantic ridge. *Contrib. Mineral. Petrol*. 96, 121–139.

Tsuchiyama, A. (1986). Melting and dissolution kinetics: application to partial melting and dissolution of xenoliths. *J. Geophys. Res*. 91, 9395–9406. doi: 10.1029/JB091iB09p09395

Ulmer, P. (1989). The dependence of the Fe2+-Mg cation-partitioning between olivine and basaltic liquid on pressure, temperature and composition. *Contrib. Mineral. Petrol.* 101, 261–273. doi: 10.1007/BF00375311

Villiger, S., Ulmer, P., and Müntener, O. (2007). Equilibrium and fractional crystallization experiments at 0.7 GPa; the effect of pressure on phase relations and liquid compositions of tholeiitic magmas. *J. Petrol.* 48, 159–184. doi: 10.1093/petrology/egl058

White, R. S., Redfern, S. A. T., and Chien, S.-Y. (2012). Episodicity of seismicity accompanying melt intrusion into the crust. *Geophys. Res. Lett.* 39:L08306. doi: 10.1029/2012GL051392

Williams, C. M. (2007). *Oceanic Lithosphere Magnetization: Marine Magnetic Investigations of Crustal Accretion and Tectonic Processes in Mid-Ocean Ridge Environments.* Ph.D. thesis, Massachusetts Institute of Technology, Woods Hole Oceanographic Institution, Woods Hole, MA.

Wood, B. J., and Blundy, J. D. (1997). A predictive model for rare earth element partitioning between clinopyroxene and anhydrous silicate melt. *Contrib. Mineral. Petrol.* 129, 166–181. doi: 10.1007/s004100050330

Conflict of Interest Statement: The authors declare that the research was conducted in the absence of any commercial or financial relationships that could be construed as a potential conflict of interest.